https://doi.org/10.5194/hess-2019-397
Preprint. Discussion started: 15 August 2019
© Author(s) 2019. CC BY 4.0 License.

Hydrology and Earth System Sciences
Discussions
Open Access

Impact of revegetation of the Loess Plateau of China on the regional growing season water balance

Jun Ge[1, 2], Andrew J. Pitman[2], Weidong Guo[1, 3], Beilei Zan[4, 5], Congbin Fu[1, 3]

[1]Institute for Climate and Global Change Research, School of Atmospheric Sciences, Nanjing University, Nanjing, 210023, China.

[2]ARC Centre of Excellence for Climate Extremes and Climate Change Research Centre, University of New South Wales, Sydney, 2052, Australia.

[3]Joint International Research Laboratory of Atmospheric and Earth System Sciences, Nanjing University, Nanjing, 210023, China.

[4]Key Laboratory of Land Surface Process and Climate Change in Cold and Arid Regions, Northwest Institute of Eco-Environment and Resources, Chinese Academy of Sciences, Lanzhou, 730000, China

[5]University of Chinese Academy of Sciences, Beijing, 100049, China

Corresponding to: Congbin Fu (fcb@nju.edu.cn)

Abstract. To resolve a series of ecological and environmental problems over the Loess Plateau, the "Grain for Green Program (GFGP)" was initiated at the end of 1990s. Following the conversion of croplands and bare land on hillslopes to forests, the Loess Plateau has displayed a significant greening trend with soil erosion being reduced. However, the GFGP has also affected the hydrology of the Loess Plateau which has raised questions whether the GFGP should be continued in the future. We investigated the impact of revegetation on the hydrology of the Loess Plateau using high resolution simulations and multiple realisations with the Weather Research and Forecasting (WRF) model. Results suggests that land cover change since the launch of the GFGP has reduced runoff and soil moisture due to enhanced evapotranspiration. Further revegetation associated with the GFGP policy is likely to increase evapotranspiration further, and thereby reduce runoff and soil moisture. The increase in evapotranspiration is associated with biophysical changes, including deeper roots that deplete deep soil moisture stores. However, despite the increase in evapotranspiration our results show no impact on rainfall. Our study cautions against further revegetation over the Loess Plateau given the reduction in water available for agriculture and human settlements, without any significant compensation from rainfall.

1 Introduction

https://doi.org/10.5194/hess-2019-397
Preprint. Discussion started: 15 August 2019
© Author(s) 2019. CC BY 4.0 License.
Hydrology and Earth System Sciences
Discussions

The Loess Plateau is a highland region of north central China, covering about 640,000 km^2. The loess soils are well suited for agriculture so natural forests have been progressively converted to farmland to support the growing population over the last 7000 years (Fu et al., 2017). However, the loess is also prone to wind and water erosion, and the long history of deforestation is associated with soil erosion, resulting in land degradation, low agricultural productivity and significant local poverty in some farming communities (Bryan et al., 2018; Chen et al., 2015; Fu et al., 2017). The soil erosion aggravates the flux of sediment into the Yellow River (Fu et al., 2017; Miao et al., 2010; Peng et al., 2010) increasing the risk of catastrophic flooding in some densely populated regions downstream (Bryan et al., 2018; Chen et al., 2015; Fu et al., 2017).

To minimise soil erosion, mitigate flood risk, store carbon and improve livelihoods over the Loess Plateau, the "Grain for Green Program (GFGP)" was initiated by reforesting hillslopes in the late 1990s (Bryan et al., 2018; Fu et al., 2017; Liu et al., 2008). Consequently, the Loess Plateau has displayed a "greening" trend (Fu et al., 2017; Li et al., 2017). The large scale vegetation restoration program has also reduced soil erosion over the Loess Plateau and alleviated sediment transport into the Yellow River (Fu et al., 2017; Liang et al., 2015; Miao et al., 2010; Peng et al., 2010; Wang et al., 2016).

As a consequence of the beneficial outcomes of the GFGP, further investment is planned with a commitment of around $US33.9 billion by China through to 2050 (Feng et al., 2016). However, further revegetation over the Loess Plateau is controversial (Cao et al., 2011; Chen et al., 2015; Fu et al., 2017) with evidence from field (Jia et al., 2017; Jin et al., 2011; Wang et al., 2012) and satellite (Feng et al., 2017; Lv et al., 2019a; Xiao, 2014) observations that revegetation has affected the hydrological balance of the region. Compared with croplands or barren surfaces, the planted forests enable higher evapotranspiration associated with a larger leaf area, higher aerodynamic roughness and deeper roots (Anderson et al., 2011; Bonan, 2008; Bright et al., 2015). Consequently, revegetation tends to decrease soil moisture and runoff with the associated risk of limiting water availability for agriculture, human consumption and industry (Cao et al., 2011; Chen et al., 2015; Fu et al., 2017). Indeed, the present vegetation over the Loess Plateau, which reflects decades of reafforestation, may already exceed the limit that the local water supply can support, and hence further revegetation may not be sustainable (Feng et al., 2016; Zhang et al., 2018).

https://doi.org/10.5194/hess-2019-397
Preprint. Discussion started: 15 August 2019
© Author(s) 2019. CC BY 4.0 License.

Hydrology and Earth System Sciences
Discussions

The impact of revegetation on evapotranspiration, soil moisture and runoff over the Loess Plateau has been studied; however the response of rainfall to large-scale revegetation is rarely investigated. As an important component of hydrological cycle, rainfall not only controls the terrestrial water budget, but also influences soil erosion and the discharge of sediment into the Yellow River (Liang et al., 2015; Miao et al., 2010; Peng et al., 2010; Wang et al., 2016). Therefore, how rainfall responds to revegetation is critical to a comprehensive assessment of the impact of revegetation on the hydrology of the region. Indeed, if rainfall responds to revegetation, this may influence national policies on whether to continue large scale vegetation restoration programs. Afforestation or deforestation does have the potential to affect rainfall via changes in biogeophysical processes, but any impact of reforestation on rainfall tends to be highly regionally specific (Chen and Dirmeyer, 2017; Quesada et al., 2017).

Several studies have used coupled models to assess the hydrological impact of revegetation across China (Cao et al., 2017; Li et al., 2018). Lv et al. (2019b) examined revegetation over the Loess Plateau and found an increase in the simulated rainfall. Li et al. (2018) also reported a positive feedback of rainfall to revegetation over North China (covering but not limited to the Loess Plateau), which was large enough to compensate for the increase in evapotranspiration and resulted in little impact on soil moisture. This simulated negligible soil moisture change associated with revegetation is contradicted by studies based on observations (e.g., Feng et al., 2017; Jia et al., 2017; Wang et al., 2012). Thus, the impact of revegetation on the hydrology of the Loess Plateau remains unclear due to the uncertainty in the rainfall response. Moreover, as far as we know, there has been no study investigating how the regional hydrology would be affected if further revegetation was undertaken.

In this study, we examine the impact of revegetation following the launch of the GFGP on the hydrology of the Loess Plateau using high resolution simulations with the Weather Research and Forecasting model. We also examine the impact of further revegetation on the hydrology of the Loess Plateau with the goal of providing helpful information to policy makers. We pay particular attention to the response of rainfall to revegetation, which is rarely available from observations.

■ 2 Methods

■ 2.1 Model configuration

The Weather Research and Forecasting (WRF, version 3.9.1.1, Skamarock et al., 2008), a fully coupled land-atmosphere regional weather and climate model, was used in our study. To perform simulations at high spatial

https://doi.org/10.5194/hess-2019-397
Preprint. Discussion started: 15 August 2019
© Author(s) 2019. CC BY 4.0 License.

Hydrology and Earth System Sciences
Discussions
Open Access

resolution over the Loess Plateau region, we applied two-way nested runs, with two domains at different grid resolutions running simultaneously. The ERA-Interim reanalysis data (Dee et al., 2001, Table 1) provided the boundary conditions for the larger and coarser resolution (30 km) domain, and the larger domain provided boundary conditions for the smaller and higher resolution (10 km) domain. The ERA-Interim reanalysis data also provided the initial conditions for both domains. Using a lambert projection, the larger domain was centred at 100°E, 37°N, with 180 grid points in west-east direction and 155 grid points in south-north direction, covering most of China and some surrounding regions (Fig. 1a). The inner domain covers the entire Loess Plateau with 166 grid points in west-east direction and 151 grid points in south-north direction (Fig. 1a and 1b). Both domains had 28 sigma levels in vertical direction with the top level set at 70 hPa. Figure 1b shows the region analysed in this paper.

The main physical parameterization schemes used in our study included the WRF Single-Moment 6-class scheme (Hong and Lin, 2006) for microphysics, the Dudhia scheme (Dudhia, 1989) for shortwave radiation, the Rapid Radiative Transfer Model (RRTM, Mlawer et al., 1997) for longwave radiation, a revised MM5 scheme (Jimenez et al., 2012) for the surface layer, the Noah Land Surface Model (Ek, 2003), the Yonsei University scheme (Hong et al., 2006) for the planetary boundary layer, and the Kain-Fritsch scheme (Kain, 2004) for cumulus convection. The Noah Land Surface Model used the Unified NCEP/NCAR/AFWA scheme with soil temperature and moisture in four layers (1st layer: 0-10 cm, 2nd layer: 10-40 cm, 3rd layer: 40-100 cm, 4th layer: 100-200 cm), fractional snow cover and frozen soil physics. A sub-tiling option considering three land cover types within each grid cell was applied to help improve the simulations of the land surface fluxes and temperature (Li et al., 2013).

2.2 Data

2.2.1 Satellite data

We used satellite observed land cover data obtained from the Moderate Resolution Imaging Spectroradiometer (MODIS) Land Cover Type product (MCD12Q1, Version 6, Friedl and Sulla-Menashe, 2019, Table1). This provides land cover types based on International Geosphere-Biosphere Program (IGBP) classification scheme (Table 2) globally at a spatial resolution of 500 m, and at yearly intervals from 2001 to 2017. The MCD12Q1 Version 6 is improved over previous versions via substantial improvements to algorithms, classification schemes and spatial resolution (Sulla-Menashe et al., 2019). The MCD12Q1 data were reprojected to Geographic Grid data with a resolution of 30 second (approximately 0.9 km) by the MODIS Reprojection Tool to make them suitable for WRF.

Key land surface biogeophysical parameters include the green vegetation fraction (*VEGFRA*), snow free albedo (α), leaf area index (*LAI*), and the background roughness length (Z_0). The fraction of Photosynthetically Active Radiation (*FPAR*) can be used as a proxy of *VEGFRA* (Kumar et al., 2014; Liu et al., 2006) enabling both *VEGFRA* and *LAI* data to be obtained from the MODIS Terra+Aqua LAI/FPAR product (MCD15A2H, Version 6, Myneni et al., 2015a, Table 1). This provides 8-day composite *LAI* and *FPAR* globally at a spatial resolution of 500 m since 4th July, 2002. The MODIS Terra LAI/FPAR product (MOD15A2H, Version 6, Myneni et al., 2015b, Table 1) was also used to provide observations prior to 2002 as it started on 8th February, 2000. Although MOD15A2H has a longer span time, MCD15A2H is generally preferred. This is because only observations from the MODIS sensor on NASA's Terra satellite is used to generate MOD15A2H, but observations from sensors on both Terra and Aqua satellites are used for MCD15A2H. The MCD15A2H and MOD15A2H Sinusoidal Tile Grid data were reprojected before use. The 8-day *LAI* and *FPAR* data were composited to monthly data to make them suitable for WRF.

As we only focus the growing season (see Section 2.3.1), α can be assumed to be equivalent to satellite observed snow-free albedo. The α data was derived from the blue sky albedo for shortwave provided by the Global Land Surface Satellite (GLASS) product (Liang and Liu, 2012, Table 1). This provides an 8-day composite albedo globally at a spatial resolution of 0.05° from 1981 to present. Compared with the MODIS albedo product, the GLASS albedo product has a higher temporal resolution and captures the surface albedo variations better (Liu et al. 2013). The 8-day α data were composited to monthly data.

The background roughness length (Z_0) was calculated following Eq. (1):

$$Z_0 = Z_{min} + \frac{VEGFRA - VEGFRA_{min}}{VEGFRA_{max} - VEGFRA_{min}} \times (Z_{max} - Z_{min}) \quad (1)$$

where Z_{max} and Z_{min} were land cover dependent maximum and minimum background roughness length respectively, provided by lookup tables. *VEGFRA*, $VEGFRA_{max}$ and $VEGFRA_{min}$ are the instantaneous, maximum and minimum green vegetation fraction, which were calculated from satellite observed *VEGFRA* (equal to *FPAR*) which would be implemented in WRF (see Section 2.3).

2.2.2 Observation data

To evaluate the WRF model performance in simulating the surface air temperature and rainfall over the Loess Plateau, we used a gridded observation dataset developed by the National Meteorological Information Centre of the China Meteorological Administration (Zhao et al., 2014, Table 1). The dataset provides monthly surface air temperature and rainfall at a spatial resolution of 0.5° from 1961 to present and was produced by merging more than 2400 station observations across China using Thin Plate Spline interpolation. The dataset has been widely used to analyse the surface air temperature and rainfall over the Loess Plateau (Sun et al., 2015; Tang et al., 2018). To facilitate the comparison between simulations and observations, the observation data were bilinearly interpolated to the WRF inner domain grid.

2.3 Experiment design

2.3.1 The impact of land cover change since the launch of the GFGP

To examine the impact of land cover change on the hydrology of the Loess Plateau since the launch of the GFGP we conducted a control experiment (LC_{2001}) and a sensitivity experiment (LC_{2015}). For the LC_{2001}, satellite observed land cover, *VEGFRA*, *LAI* and α in 2001 were used to approximate land cover and land surface biogeophysical parameters before the launch of the GFGP. There is a one-year gap between the launch of the GFGP (end of 1999) and 2001, but any bias introduced by this gap is small compared with the changes in land surface biogeophysical parameters between 1999 and present. Satellite observed land cover, *VEGFRA*, *LAI* and α in 2015, representing the current land cover and land surface biogeophysical status, were used for the LC_{2015}. Model configurations were identical for the LC_{2001} and LC_{2015} except for land cover and land surface biogeophysical parameters. Comparing the LC_{2001} and LC_{2015} therefore isolates the impact of land cover change since the launch of the GFGP.

We note land cover change here, rather than revegetation or afforestation, for two reasons. First, actual land cover changes since the launch of the GFGP are highly spatially heterogeneous. MCD12Q1 suggests that most land cover changes have occurred in the south Loess Plateau (SLP, 105-111°E, 35-37°N) and east Loess Plateau (ELP, 111-114°E, 35-39°N) (Fig. 2a, 2c, 2e and 2g). In addition to the gain of forests (including evergreen needleleaf, evergreen broadleaf, deciduous needleleaf, deciduous broadleaf and mixed forests) and savannas (including woody savannas and savannas), other land cover changes include the expansion of croplands (including croplands

© Author(s) 2019. CC BY 4.0 License.

and cropland/natural vegetation mosaics) at the expense of grasslands and savannas (Fig. 2g). Second, the observed *VEGFRA*, *LAI* and α changes also incorporate other factors including improved agricultural management, climate variability, rising atmospheric CO_2 concentration and nitrogen deposition (Li et al., 2017; Piao et al., 2015). As shown in Fig. 3a, 3c, 3e, and 3g, the biogeophysical changes are not strictly limited to the regions undergoing land cover change. For example, the α change mostly occurs over grasslands in northwest (Fig. 3e), where land cover changes are less intense (Fig 2c). Overall however, the MCD12Q1 demonstrates a significant greening trend (increased *VEGFRA*, *LAI* and Z_0 and decreased α) over the Loess Plateau since the launch of the GFGP (Figure 3).

Both LC_{2001} and LC_{2015} were run from 1st May to 30th September for years from 1996 to 2015 resulting in twenty realisation members for each of LC_{2001} and LC_{2015}. We only run for the growing season; any impact of reforestation should be most apparent during the growing season given that over 70% of the annual rainfall occurs over the Loess Plateau in this season (Sun et al., 2015; Tang et al., 2018).

■ 2.3.2 The impact of further revegetation on the Loess Plateau

If the GFGP is continued in the future, further revegetation could impact the hydrology of the Loess Plateau. We therefore conducted a third experiment (LC_{futr}) in which the coverage of forests was assumed to be maximum over the Loess Plateau following the policy of the GFGP. To maximise forests we first assumed all croplands and barren on hillslopes were converted to forests. Second, we assumed savannas or forests with low coverage (e.g., low *VEGFRA*) became dense forests. The land cover and land surface biogeophysical parameters for the LC_{futr} were then constructed following two steps.

First, all croplands, barren and savannas pixels on hillslopes ($>15^{o}$) were replaced by forests pixels over the Loess Plateau based on the land cover map of 2015. The slope is derived from the Shuttle Radar Topography Mission (SRTM version 2.0, Table 1) Digital Elevation Model at a spatial resolution of 3 second (about 90 m). The pixel resolution of the land cover is 30 second, so every land cover pixel covered 100 (10×10) slope values. To maximise the revegetation, land cover pixels with maximum slope values over 15^{o} were regarded as hillslopes. For a pixel to be changed, the forest class was determined by the class of neighbouring forests pixels, considering the adaptation of planted trees to local climate. Using this strategy, forests pixels increased by 164% and croplands

https://doi.org/10.5194/hess-2019-397
Preprint. Discussion started: 15 August 2019
© Author(s) 2019. CC BY 4.0 License.

pixels decreased by nearly a half in the constructed land cover map compared with the land cover in 2001, with most conversions occurring in SLP (Fig. 2b and 2h).

Second, we constructed the *VEGFRA*, *LAI* and α map in line with the land cover map constructed in the first step. For each forests class, we screened out the "dense forests" pixels with *VEGFRA* over the 95th percentile among the pixels labelled as the same forests class over the Loess Plateau. The monthly values of *VEGFRA*, *LAI* and α of the "dense forest" pixels were calculated for each forests class. We then adjusted the monthly *VEGFRA*, *LAI* and α of other "non-dense forests" pixels to the values of the "dense forests" pixels. Using this strategy, all forests pixels over the Loess Plateau were changed to more dense forest. Consequently, the Loess Plateau shows an amplified greening trend in LC_{futr}, especially in SLP (Fig. 3b, 3d, 3f and 3h).

The LC_{futr} was run from 1st May to 30th September for years from 1996 to 2015. Therefore comparing LC_{2001} and LC_{futr} isolates the impact of further revegetation on the hydrology of the Loess Plateau.

■ 2.3.3 Identification of the impact of revegetation

Model internal variability is defined as the difference between realisation members where the only differences are the initial conditions. These differences result from nonlinearities in the model physics and dynamics (Giorgi and Bi, 2000; Christensen et al., 2001). This means some differences between LC_{2001} and LC_{2015} (or LC_{futr}) will be caused by internal variability in addition to land cover changes (Lorenz et al., 2016; Ge et al., 2019). To minimise the impact of internal model variability we performed multiple simulations for the year 2001 by changing initial conditions. Specifically, we carried out a pair of experiments named $LCENS_{2001}$ and $LCENS_{2015}$, which were the same as LC_{2001} and LC_{2015} except that $LCENS_{2001}$ and $LCENS_{2015}$ were only run for the year 2001 but initialized for each day between 21st to 30th April, and ending on 30th September. This led to a total of eleven members (including the members with initial dates of 1st May in LC_{2001} and LC_{2015}) for $LCENS_{2001}$ and $LCENS_{2015}$ respectively. Comparing $LCENS_{2001}$ and $LCENS_{2015}$, simulated changes were likely robust if the impact from revegetation was large and consistent relative to the differences caused by the change in the initial condition.

Results before 1st June was discarded as spin-up time in each simulation. Our analysis focusses on June, July, August and September (JJAS) averages.

■ 2.5 Local significance test

https://doi.org/10.5194/hess-2019-397
Preprint. Discussion started: 15 August 2019
© Author(s) 2019. CC BY 4.0 License.

To test the statistical significance of the local impact of land cover change on the hydrology we calculate a grid-point by grid-point Student's *t*-test. This tests the null hypothesis that the two groups of data are from independent random samples from normal distributions with equal means and equal but unknown variances. The local difference is regarded as statistically significant when the *p*-value of the two-tailed *t*-test passes the significance level of 95%.

3 Results

3.1 Evaluation of WRF's skill in simulating temperature and rainfall

We first evaluate WRF's simulation of surface air temperature (*T2*) and rainfall (*RAIN*), the quantities with the most credible observations available over the Loess Plateau, using the eleven members in $LCENS_{2001}$ with the observed values in 2001. After topographic correction (Zhao et al., 2008), WRF simulates *T2* over the Loess Plateau mostly within 2°C of the observations (Fig. 4a, 4c, 4e) although there are small areas where WRF simulates warmer temperatures than the observations by 4°C. The model also performs well in simulating *RAIN* (Fig. 4b, 4d, 4f) including a region of higher observed rainfall from the southwest to the central Loess Plateau. The *RAIN* bias between the WRF simulations and the observations is below 0.5 mm/day for almost the entire Loess Plateau (Fig. 4f). Larger *RAIN* biases mostly occur around the eastern and southern borders of the Loess Plateau, most likely due to extremely complex topography in these locations. Since we focus on the impact of land cover change on the hydrology of the region, the reasonable simulation of *RAIN* gives us confidence in the results from WRF, particularly in SLP.

3.2 Impacts on surface fluxes

We first examine the change in the land surface radiation budget, energy and water fluxes as these are directly impacted by land cover and the surface biogeophysical changes. Comparing LC_{2001} and LC_{2015} (LC_{2015}-LC_{2001}), land surface net radiation (R_{net}), latent heat flux (Q_E) and sensible heat flux (Q_H) changes mainly occur where land cover and land surface biogeophysical parameters are changed, suggesting a strong local effect on R_{net}, Q_E and Q_H. R_{net} increases by around 5-20 W·m^{-2} (Fig. 5a), over most of the region due to a reduction in α (Fig. 3e). While Q_E increases by 10-30 W·m^{-2} (Fig. 5c) and Q_H reduces by around 10 W·m^{-2} (Fig. 5e), mostly in SLP and ELP as a result of increased *VEGFRA*, *LAI* and Z_0 (Fig. 3a, 3c and 3g). Changes in R_{net} and Q_E are statistically significant at a 95% confidence level over most of the region, but statistically significant changes in Q_H are mostly limited to

SLP and ELP (see the embedded subplots in each panel, Fig. 5a, 5c and 5e). As a consequence of further revegetation (LC_{futr}-LC_{2001}), R_{net}, Q_E and Q_H changes are intensified (Fig. 5b, 5d and 5f), especially in SLP where large areas of croplands are converted to forest leading to large changes in land surface biogeophysical parameters in LC_{futr} (Fig. 2 and 3).

Focusing on SLP, the increase in evapotranspiration (*ET*) is 0.49 mm·day^{-1} between LC_{2001} and LC_{2015} (Fig. 6a). WRF simulates further water loss (0.85 mm·day^{-1}) through *ET* if the revegetation is continued in the future (Fig. 6c). For ELP, where relative fewer croplands or barren can be further converted to forests in LC_{futr}, the future *ET* increase is still considerable (0.72 mm·day^{-1}, Fig. 6b and 6d). The values of regional mean *ET* change among the twenty members of LC_{2015}-LC_{2001} and LC_{futr}-LC_{2001} remain consistently positive over SLP and ELP. This indicates that the simulated higher *ET* is a consistent result from WRF as a consequence of the land cover changes since the launch of the GFGP, and is likely to be further strengthened by continued revegetation over the Loess Plateau.

■ 3.3 Impacts on rainfall

Increased *ET* can contribute to the formation of clouds and rainfall, and we therefore examine whether this is the case for the Loess Plateau. The *RAIN* is composed of convective rainfall (*RAINC*) calculated by the cumulus convection scheme, and non-convective rainfall (*RAINNC*) calculated by microphysics scheme in WRF. Thus we separate *RAINC* and *RAINNC* changes in addition to the *RAIN* change in Fig.7. As for LC_{2015}-LC_{2001}, the change in *RAIN* is spatially heterogeneous, with an increase of up to 1.2 mm·day^{-1} in small parts of the northeast and a decrease around -1.0 mm·day^{-1} along the southeast border of the Loess Plateau (Fig. 7a). The *RAIN* change is divided almost evenly between *RAINC* and *RAINNC* (Fig. 7c and 7e). However, the *RAIN*, *RAINC* and *RAINNC* changes are not statistically significant. In terms of LC_{futr}-LC_{2001}, *RAIN*, *RAINC* and *RAINNC* are not significantly changed by further revegetation (Fig. 7b, 7d and 7f). Moreover, the increased rainfall in northeast Loess Plateau occurring in LC_{2015}-LC_{2001} dissipate when further revegetation is implemented suggesting that this change is largely associated with internal model variability.

For both LC_{2015}-LC_{2001} and LC_{futr}-LC_{2001} cases, most *RAIN* changes seems to be randomly scattered around the Loess Plateau instead of being located coincident with SLP or ELP where land cover, land surface biogeophysical parameters and land surface fluxes are most strongly modified (Fig. 7a and 7b). The *RAIN* change is negligible over SLP and ELP for both LC_{2015}-LC_{2001} and LC_{futr}-LC_{2001} cases (Fig. 6 and 7). However, the *RAIN* change in

https://doi.org/10.5194/hess-2019-397
Preprint. Discussion started: 15 August 2019
© Author(s) 2019. CC BY 4.0 License.

individual realisations is not small, e.g., the *RAIN* change varies from -2.11 to 2.21 mm·day^{-1} over the ELP for LC$_{2015}$-LC$_{2001}$ (Fig. 6b). So averaging the divergent *RAIN* changes among the twenty members causes a negligible *RAIN* change overall. This large variability in *RAIN* changes among the twenty members can be attributed to either different boundary conditions (background climate), which causes the impact of land cover change to diverge (Pitman et al., 2011), or model internal variability. This will be further analysed in Section 3.6.

■ 3.4 Impacts on runoff

As a consequence of the significant *ET* increase and negligible and statistically insignificant *RAIN* change, underground runoff (*UDROFF*) is reduced by up to 1.5 mm·day^{-1} locally for LC$_{2015}$-LC$_{2001}$ (Fig 8c). Averaged over the SLP and ELP, the *UDROFF* decreases by 0.16 mm·day^{-1} (-23%) and 0.34 mm·day^{-1} (-23%) for SLP and ELP respectively (Fig. 6a and 6b). These *UDROFF* changes are not statistically significant and vary strongly among the twenty members, suggesting a large uncertainty in the *UDROFF* change. WRF simulated a larger *UDROFF* decrease due to further revegetation (Fig. 8d), especially over SLP and ELP where the regional mean *UDROFF* decreases by 0.38 mm·day^{-1} (-54%) and 0.63 (-42%) respectively (Fig. 6c and 6d). These *UDROFF* decreases are statistically significant at a 95% confidence level for both SLP and ELP. Moreover, the upper quartile of *UDROFF* changes among the twenty members systematically shift below the 0 mm·day^{-1} value for both the SLP and ELP. These results indicate a larger chance of the *UDROFF* decrease if the revegetation is continued over the SLP and ELP. We also note some *UDROFF* changes in adjacent regions of the Loess Plateau (Fig. 8c and 8d) associated with *RAIN* changes (Fig. 7a and 7b).

Compared with the *UDROFF* change, the surface runoff (*SUROFF*) change are mostly small for both LC$_{2015}$-LC$_{2001}$ and LC$_{futr}$-LC$_{2001}$ (Fig. 8a and 8b). However, the relative change of *SUROFF* is considerable, especially for the LC$_{futr}$-LC$_{2001}$ case in which *SUROFF* decreased by 21% for the SLP and 14% for the ELP respectively (Fig. 6c and 6d). We also find the upper quartile of the *SUROFF* change systematically shifts below the 0 mm·day^{-1} value although the *SUROFF* change are not statistically significant for the LC$_{futr}$-LC$_{2001}$.

■ 3.5 Impacts on soil moisture

In addition to the decline in runoff, the soil moisture (*SMOIS*) of each layer is significantly reduced over the Loess Plateau for LC$_{2015}$-LC$_{2001}$ (Fig. 9a, 9c, 9e and 9g) with larger decreases in the middle two layers. The regional mean *SMOIS* for the SLP decreases by 0.02 m·m^{-3} (-8%) and 0.03 m·m^{-3} (-12%) for the second and third layers.

https://doi.org/10.5194/hess-2019-397
Preprint. Discussion started: 15 August 2019
© Author(s) 2019. CC BY 4.0 License.
Hydrology and Earth System Sciences Discussions

WRF simulated further falls in soil moisture following further revegetation, with a larger impact on deeper soil layer moisture (Fig. 9b, 9d, 9f and 9h). For example, the decrease in regional mean soil moisture of the bottom layer for the SLP varies from -0.01 (or -5%) in LC_{2015}-LC_{2001} to -0.04 (or -17%) in LC_{futr}-LC_{2001}.

■ 3.6 Robust identification of rainfall change

We found a large variability in changes in *RAIN* among the twenty members over the SLP and ELP for both LC_{2015}-LC_{2001} and LC_{futr}-LC_{2001}. We next examine whether these can be attributed to land cover change. We first show the *RAIN* change in individual members for LC_{2015}-LC_{2001} (Fig. 10). The large variability of *RAIN* changes among the twenty members occur throughout the study region. Even the increase in *RAIN* over the northeast Loess Plateau (Fig. 7a), which is available by comparing multiyear mean *RAIN* between LC_{2001} and LC_{2015}, is not consistent for every year. As for the northeast Loess Plateau, the *RAIN* shows an increase in 8 years (1997, 2001, 2003, 2004, 2007, 2010, 2012 and 2015), decrease in 5 years (1996, 1999, 2006, 2009 and 2014) and negligible changes in other 7 years. This results in a net increase in *RAIN* over the twenty years, but a different selection of years could show an overall decrease (the result is similar for LC_{futr}-LC_{2001}, not shown).

We note that the pattern of *RAIN* change in 2001 is very similar to the multiyear averaged one, but with a larger magnitude (cf. Fig. 7a and 10f). The *RAIN* increase of the northeast Loess Plateau in just 2001 explains about 30% of the multiyear mean *RAIN* increase in the same region. We therefore show the *RAIN* change in each realisation for $LCENS_{2015}$-$LCENS_{2001}$ in Fig. 11 to highlight that the changes are not consistent among the eleven ensemble members despite their sharing the same boundary conditions. For example, WRF cannot simulate the increased *RAIN* over northeast Loess Plateau when using an initial date of 22nd, 25th, 27th and 30th April highlighting that the *RAIN* change is very sensitive to the initial conditions. Thus, the *RAIN* increase in 2001 with an initial date of 1st May is likely associated with internal variability rather than land cover change. We therefore conclude that the multiyear averaged *RAIN* change over northeast Loess Plateau for LC_{2015}-LC_{2001} (Fig. 7a) cannot be robustly linked with land cover change.

■ 3.7 How many members do we need to get a robust signal?

Model internal variability is inevitable when we use models to investigate the impact of land cover change on climate. The model internal variability can be minimised as the number of individual realisations is increased to form a larger sample to calculate any average. We therefore examine the relationship between the *RAIN* change

https://doi.org/10.5194/hess-2019-397
Preprint. Discussion started: 15 August 2019
© Author(s) 2019. CC BY 4.0 License.

and the number of realisation members (Fig. 12). Focusing on the SLP and ELP, the range of *RAIN* change decreases as the number of realisations increase. For example, the *RAIN* change over the ELP varies from -0.97 to 1.07 mm·day^{-1} when only three members are included. The range of *RAIN* is narrowed to between -0.25 and 0.24 mm·day^{-1} when fifteen members are simulated. It is similar for LCENS_{2015}-LCENS_{2001}; the range in the change in *RAIN* decreases as the number of simulation members increases. The change in *RAIN* suggests an increase of 0.48 and 0.40 mm·day^{-1} for the SLP and ELP respectively when the simulation members are increased to eleven.

■ 4 Discussion

Following the launch of the GFGP by China in the late 1990s, the Loess Plateau has shown a significant greening trend, but with simultaneous concerns about water security for agriculture and other human activities. We investigated the impact of land cover change since the launch of the GFGP on the hydrology of the Loess Plateau using WRF. Simulations show that the revegetation of the plateau is associated with a decrease in runoff and soil moisture as a consequence of higher evapotranspiration.

Our results are broadly consistent with both field (Jia et al., 2017; Jian et al., 2015; Jin et al., 2011) and satellite (Feng et al., 2017; Li et al., 2016; Xiao, 2014) observations. For example, the spatial pattern of our simulated soil moisture decline in the growing season is similar to observations from the Advanced Microwave Scanning Radiometer on the Earth Observing System by the Japanese Aerospace Exploration Agency (Feng et al., 2017). Observations of soil moisture declines associated with revegetation are not always permanent and may be alleviated once trees exceed 25 years (Jia et al., 2017; Jin et al., 2011). Our simulations only capture the initial decline in runoff and soil moisture linked with the higher evapotranspiration and we note that the impact of revegetation on the long-time trend (25 - 50 years) would be valuable.

We also investigated the potential future impact on the hydrology of the Loess Plateau if revegetation was continued. WRF suggests that further revegetation would exacerbate soil moisture and runoff declines with particularly large effects on the underground runoff and soil moisture in deeper layers. Our simulations suggested that the potential revegetation that could still be achieved would have larger consequences than those simulated since the launch of the GFGP. However, we note some limitations in our experiment design. First we use current boundary conditions (1996-2015) to drive WRF, which means the background climate does not change in the future in response to climate change. Second, uncertainties exist in the current land surface model used to represent the response of vegetation to climate change in future. While using satellite observations to construct the land surface biogeophysical parameters helps overcome some land surface parameter limitations, this approach is obviously limited looking forward in terms of the status of future vegetation. Despite these limitations, our results provide useful advances in our understanding of the impact of revegetation on the Loess Plateau. For example, both Feng et al. (2016) and Zhang et al. (2018) estimated the current vegetation over the Loess Plateau is approaching or may have exceeded the threshold of ecological equilibrium. They omitted the potential response of rainfall to further revegetation over the Loess Plateau when predicting future thresholds (Feng et al., 2016; Zhang et al., 2018). Our result demonstrate that there is almost no feedback of rainfall associated with further revegetation, supporting the approach of Feng et al. (2016) and Zhang et al. (2018) in this specific region. That said, our approach does not attempt to incorporate changes in climate over the Loess Plateau and so the viability of large-scale reforestation in this region is not something we attempted to assess.

We focused on the response of rainfall to revegetation over the Loess Plateau, which is probably the most uncertain of the hydrological components. WRF shows little response of rainfall to the land cover change since the launch of the GFGP. Moreover, the rainfall is weakly affected by further revegetation despite large increase in evapotranspiration. We also demonstrate that the rainfall change is strongly affected by internal variability and a large number of realisations are required before any impact of land cover change on rainfall might be robustly identified. We suggest that some previous studies (Cao et al., 2017; Lv et al., 2019) based on model simulations may have exaggerated the impact of land cover change on rainfall over the Loess Plateau due to the lack of sufficient realisations. For example, Cao et al. (2017) and Lv et al. (2019) used the WRF to perform only three and five member simulations, and concluded a significant increase in rainfall caused by land cover change over the Loess Plateau. We could also demonstrate large changes in rainfall over the plateau if we chose 3-5 members but we could demonstrate either large increases or large decreases in 3-5 member averages. Clearly, a robust result requires internal model variability to be thoroughly addressed.

We note that our results are likely model dependant as we only used one model. Although we performed high resolution (10 km for the nested domain), the cumulus convection scheme remains necessary which is a further potential source of uncertainty. These factors account for the discrepancy between our result and another model

https://doi.org/10.5194/hess-2019-397
Preprint. Discussion started: 15 August 2019
© Author(s) 2019. CC BY 4.0 License.

based study (Li et al., 2018) which found a positive rainfall feedbacks to greening over north China using a Global Climate Model. A large ensemble of models, each with a reasonable number of realisations, is needed to build a model independent assessment of the impact of revegetation but this is clearly beyond the scope of this study.

Overall, our results highlight how the GFGP led to a greening of the Loess Plateau, how this increased evapotranspiration and how as a consequence the runoff and soil moisture declined. This is consistent with the understanding of land-surface processes and how they respond to land cover change (Bonan, 2008). Critical in this impact of revegetation on the hydrology is what happens to rainfall. If the higher evapotranspiration increases rainfall, then revegetation has the potential to increase soil moisture and runoff. It is very likely this would be the consequences in some regions such as Amazonia (Lawrence and Vandecar, 2015; Perugini et al., 2017; Spracklen et al., 2018). However, over the Loess Plateau we find no such result and thus the higher evapotranspiration simply leads to lower soil moisture and runoff. An implication of this result is that further revegetation, which requires water to be sustained, may not be viable. We also recognize that afforestation can help to sequester carbon, mitigate warming and alleviate soil erosion. Therefore whether and how to implement further revegetation should be cautiously determined with the pros and cons of afforestation being carefully weighted for the Loess Plateau.

■ 5 Conclusions

We evaluated how the growing season hydrology of the Loess Plateau is impacted by revegetation since the launch of the “Grain for Green Program”, and by further revegetation in the future using the WRF model. We used satellite observations to describe key biophysical parameters including decreased albedo and increased leaf area index and fraction of photosynthetically active radiation. The observed greening trend increased evapotranspiration but because the impact on rainfall was negligible the underground runoff and soil moisture both decreased. Further future revegetation enhanced evapotranspiration, but still had little impact on rainfall. Overall therefore, revegetation over the Loess Plateau leads to higher evapotranspiration, and as a consequence lower water availability for agriculture or other human demands. Considering the negative impact of revegetation on runoff and soil moisture, and the lack of benefits on rainfall, we caution that further revegetation may threaten local water security over the Loess Plateau.

Code and data availability. The MODIS land cover type product (MCD12Q1) and LAI/FPAR products (MCD15A2H and MOD15A2H) are available on NASA’s Land Processes Distributed Active Archive Center (LP

© Author(s) 2019. CC BY 4.0 License.
Hydrology and Earth System Sciences
Discussions

DAAC), https://lpdaac.usgs.gov/data/. The GLASS albedo product is available on Global land surface satellite (GLASS) products download and service, http://glass-product.bnu.edu.cn/. The ERA-Interim reanalysis data is available on the ECMWF Data Server, https://www.ecmwf.int/en/forecasts/datasets/reanalysis-datasets/era-interim. The gridded observation dataset is available on the National Meteorological Information Centre of the China Meteorological Administration, http://data.cma.cn/data/cdcindex.html. The code of Weather Research and Forecasting model is available on http://www2.mmm.ucar.edu/wrf/users/.

Author contributions. CF, JG and WG led the overall scientific questions and designed the research. JG, AJP and BZ analysed the data and wrote the manuscript. All authors contributed to the discussion of the results and to revising the manuscript.

Competing interest. The authors declare that they have no conflict of interest.

Acknowledgements. This work was supported by the Natural Science Foundation of China (41775075, 41475063) and the Australian Research Council via the Centre of Excellence for Climate Extremes (CE170100023). This work is also supported by the Jiangsu Collaborative Innovation Center for Climate Change. The model simulations were conducted on the NCI National Facility at the Australian National University, Canberra. The authors also gratefully acknowledge financial support from China Scholarship Council.

References

Anderson, R. G., Canadell, J. G., Randerson, J. T., Jackson, R. B., Hungate, B. A., Baldocchi, D. D., Ban-Weiss, G. A., Bonan, G. B., Caldeira, K., Cao, L., Diffenbaugh, N. S., Gurney, K. R., Kueppers, L. M., Law, B. E., Luyssaert, S., O'Halloran, T. L.: Biophysical considerations in forestry for climate protection, Front. Ecol. Environ., 9, 174-182, https://doi.org/10.1890/090179, 2011.

Bonan, G. B.: Forests and climate change: Forcings, feedbacks, and the climate benefits of forests, Science, 320, 1444-1449, https://doi.org/10.1126/science.1155121, 2008.

Bright, R. M., Zhao, K. G., Jackson, R. B., Cherubini, F.: Quantifying surface albedo and other direct biogeophysical climate forcings of forestry activities, Global Change Biol., 21, 3246-3266, https://doi.org/10.1111/gcb.12951, 2015.

https://doi.org/10.5194/hess-2019-397
Preprint. Discussion started: 15 August 2019
© Author(s) 2019. CC BY 4.0 License.

Bryan, B. A., Gao, L., Ye, Y. Q., Sun, X. F., Connor, J. D., Crossman, N. D., Stafford-Smith, M., Wu, J. G., He, C. Y., Yu, D. Y., Liu, Z. F., Li, A., Huang, Q. X., Ren, H., Deng, X. Z., Zheng, H., Niu, J. M., Han, G. D., and Hou, X. Y.: China's response to a national land-system sustainability emergency, Nature, 559, 193-204. https://doi.org/10.1038/s41586-018-0280-2, 2018.

Cao, Q., Yu, D. Y., Georgescu, M., and Wu, J. G.: Substantial impacts of landscape changes on summer climate with major regional differences: The case of China, Sci. Total Environ., 625, 416-427, https://doi.org/10.1016/j.scitotenv.2017.12.290, 2017.

Cao, S. X., Chen, L., Shankman, D., Wang, C. M., Wang, X. B., and Zhang, H.: Excessive reliance on afforestation in China's arid and semi-arid regions: Lessons in ecological restoration, Earth-Sci. Rev, 104, 240-245, https://doi.org/10.1016/j.earscirev.2010.11.002, 2011.

Chen, Y. P., Wang, K. B., Lin, Y. S., Shi, W. Y., Song, Y., and He, X. H.: Balancing green and grain trade, Nat. Geosci., 8, 739-741, https://doi.org/10.1038/ngeo2544, 2015.

Chen, L. and Dirmeyer, P. A.: Impacts of Land-Use/Land-Cover Change on Afternoon Precipitation over North America, J. Climate, 30, 2121-2140, https://doi.org/10.1175/JCLI-D-16-0589.1, 2017.

Christensen, O. B., Gaertner, M. A., Prego, J. A. and Polcher, J.: Internal variability of regional climate models, Clim. Dynam., 17, 875-887, https://doi.org/10.1007/s003820100154, 2001.

Dee, D. P., Uppala, S. M., Simmons, A. J., Berrisford, P., Poli, P., Kobayashi, S., Andrae, U., Balmaseda, M. A., Balsamo, G., Bauer, P., Bechtold, P., Beljaars, A. C. M., van de Berg, L., Bidlot, J., Bormann, N., Delsol, C., Dragani, R., Fuentes, M., Geer, A. J., Haimberger, L., Healy, S. B., Hersbach, H., Holm, E. V., Isaksen, L., Kallberg, P., Kohler, M., Matricardi, M., McNally, A. P., Monge-Sanz, B. M., Morcrette, J. J., Park, B. K., Peubey, C., de Rosnay, P., Tavolato, C., Thepaut, J. N., and Vitart, F.: The ERA-Interim reanalysis: Configuration and performance of the data assimilation system. Q. J. Roy. Meteor. Soc., 137, 553-597, https://doi.org/10.1002/qj.828, 2011.

Dudhia, J.: Numerical study of convection observed during the winter monsoon experiment using a mesoscale two-dimensional model, J. Atmos. Sci., 46, 3077-3107, https://doi.org/10.1175/1520-0469(1989)046<3077:NSOCOD>2.0.CO;2, 1989.

© Author(s) 2019. CC BY 4.0 License.

Ek, M. B.: Implementation of Noah land surface model advances in the National Centers for Environmental Prediction operational mesoscale Eta model, J. Geophys. Res. - Atmos., 108, 8851, https://doi.org/10.1029/2002JD003296, 2003.

Feng, X. M., Fu, B. J., Piao, S. L., Wang, S. A., Ciais, P., Zeng, Z. Z., Lu, Y. H., Zeng, Y., Li, Y., Jiang, X. H., and Wu, B. F.: Revegetation in China's Loess Plateau is approaching sustainable water resource limits, Nat. Clim. Change, 6, 1019. https://doi.org/10.1038/NCLIMATE3092, 2016.

Feng, X. M., Li, J. X., Cheng, W., Fu, B. J., Wang, Y. Q., Lu, Y. H., and Shao, M. A.: Evaluation of AMSR-E retrieval by detecting soil moisture decrease following massive dryland re-vegetation in the Loess Plateau, China, Remote Sens. Environ., 196, 253-264, https://doi.org/10.1016/j.rse.2017.05.012, 2017.

Fu, B. J., Wang, S., Liu, Y., Liu, J. B., Liang, W., and Miao, C. Y.: Hydrogeomorphic Ecosystem Responses to Natural and Anthropogenic Changes in the Loess Plateau of China, Annu. Rev. Earth Pl. Sc., 45, 223-243, https://doi.org/10.1146/annurev-earth-063016-020552, 2017.

Friedl, M. and Sulla-Menashe, D.: MCD12Q1 MODIS/Terra+Aqua Land Cover Type Yearly L3 Global 500m SIN Grid V006 [MCD12Q1], NASA EOSDIS Land Processes DAAC, https://doi.org/10.5067/MODIS/MCD12Q1.006, 2019.

Ge, J., Pitman, A. J., Guo, W. D., Wang, S. Y. and Fu, C. B.: Do Uncertainties in the Reconstruction of Land Cover Affect the Simulation of Air Temperature and Rainfall in the CORDEX Region of East Asia? J. Geophys. Res. - Atmos., 124, 3647-3670. https://doi.org/10.1029/2018JD029945, 2019.

Giorgi, F. and Bi, X. Q.: A study of internal variability of a regional climate model, J. Geophys. Res. - Atmos., 105, 29503-29521, https://doi.org/10.1029/2000JD900269, 2000.

Hong, S. Y., and Lim, J. O. J.: The WRF Single-Moment 6-Class Microphysics Scheme (WSM6), J. Kor. Meteorol. Soc., 42, 129-151, 2006.

Hong, S. Y., Noh, Y., and Dudhia, J.: A new vertical diffusion package with an explicit treatment of entrainment processes, Mon. Weather Rev., 134, 2318-2341, https://doi.org/10.1175/MWR3199.1, 2006.

Jia, X. X., Shao, M. A., Zhu, Y. J., and Luo, Y.: Soil moisture decline due to afforestation across the Loess Plateau, China, J. Hydrol., 546, 113-122, https://doi.org/10.1016/j.jhydrol.2017.01.011, 2017.

https://doi.org/10.5194/hess-2019-397
Preprint. Discussion started: 15 August 2019
© Author(s) 2019. CC BY 4.0 License.

Jian, S. Q., Zhao, C. Y., Fang, S. M., and Yu, K.: Effects of different vegetation restoration on soil water storage and water balance in the Chinese Loess Plateau, Agr. Forest Meteorol., 206, 85-96, https://doi.org/10.1016/j.agrformet.2015.03.009, 2015.

Jimenez, P. A., Dudhia, J., Gonzalez-Rouco, J. F., Navarro, J., Montavez, J. P., and Garcia-Bustamante, E.: A Revised Scheme for the WRF Surface Layer Formulation, Mon. Weather Rev., 140, 898-918, https://doi.org/10.1175/MWR-D-11-00056.1, 2012.

Jin, T. T., Fu, B. J., Liu, G. H., and Wang, Z.: Hydrologic feasibility of artificial forestation in the semi-arid Loess Plateau of China, Hydrol. Earth Syst. Sc., 15, 2519-2530, https://doi.org/10.5194/hess-15-2519-2011, 2011.

Kain, J. S.: The Kain-Fritsch convective parameterization: An update, J. Appl. Meteorol. Clim., 43, 170-181, https://doi.org/10.1175/1520-0450(2004)043<0170:TKCPAU>2.0.CO;2, 2004.

Kumar, A., Chen, F., Barlage, M., Ek, M. B., and Niyogi, D.: Assessing Impacts of Integrating MODIS Vegetation Data in the Weather Research and Forecasting (WRF) Model Coupled to Two Different Canopy-Resistance Approaches, J. Appl. Meteorol. Clim., 53, 1362-1380, https://doi.org/10.1175/JAMC-D-13-0247.1, 2014.

Lawrence, D. and Vandecar, K.: Effects of tropical deforestation on climate and agriculture, Nat. Clim. Change, 5, 27-36, https://doi.org/10.1038/NCLIMATE2430, 2015.

Li, D., Bou-Zeid, E., Barlage, M., Chen, F., and Smith, J. A.: Development and evaluation of a mosaic approach in the WRF-Noah framework, J. Geophys. Res. - Atmos., 118, 11918-11935, https://doi.org/10.1002/2013JD020657, 2013.

Li, J. J., Peng, S. Z., and Li, Z.: Detecting and attributing vegetation changes on China's Loess Plateau, Agr. Forest Meteorol., 247, 260-270, https://doi.org/10.1016/j.agrformet.2017.08.005, 2017.

Li, S., Liang, W., Fu, B. J., Lu, Y. H., Fu, S. Y., Wang, S., and Su, H. M.: Vegetation changes in recent large-scale ecological restoration projects and subsequent impact on water resources in China's Loess Plateau, Sci. Total Environ., 569, 1032-1039, https://doi.org/10.1016/j.scitotenv.2016.06.141, 2016.

Li, Y., Piao, S. L., Li, L. Z. X. Chen, A. P., Wang, X. H., Ciais, P., Huang, L., Lian, X., Peng, S. S., Zeng, Z. Z., Wang, K., and Zhou, L. M.: Divergent hydrological response to large-scale afforestation and vegetation greening in China, Sci. Adv., 4, eaar4182, https://doi.org/10.1126/sciadv.aar4182, 2018.

Liang, W., Bai, D., Wang, F. Y., Fu, B. J., Yan, J. P., Wang, S., Yang, Y. T., Long, D., and Feng, M. Q.: Quantifying the impacts of climate change and ecological restoration on streamflow changes based on a

https://doi.org/10.5194/hess-2019-397
Preprint. Discussion started: 15 August 2019
© Author(s) 2019. CC BY 4.0 License.

Buddy hydrological model in China's Loess Plateau, Water Resour. Res., 51, 6500-6519. https://doi.org/10.1002/2014WR016589, 2015.

Liang, S. L. and Liu, Q.: Global Land Surface Products: Albedo Product Data Collection (1985-2010), Beijing Normal University, 2012. https://doi.org/10.6050/glass863.3001.db, 2012.

Liu, J. G., Li, S. X., Ouyang, Z. Y., Tam, C., and Chen, X. D.: Ecological and socioeconomic effects of China's policies for ecosystem services, P. Natl. Acad. Sci. USA, 105, 9477-9482, https://doi.org/10.1073/pnas.0706436105, 2008.

Liu, N. F., Liu, Q., Wang, L. Z., Liang, S. L., Wen, J. G., Qu, Y., and Liu, S. H.: A statistics-based temporal filter algorithm to map spatiotemporally continuous shortwave albedo from MODIS data, Hydrol. Earth Syst. Sc., 17, 2121-2129, https://doi.org/10.5194/hess-17-2121-2013, 2013.

Liu, Z. Y., Notaro, M., Kutzbach, J., and Liu, N.: Assessing global vegetation-climate feedbacks from observations. J. Climate, 19, 787-814, https://dopi.org/10.1175/JCLI3658.1, 2006.

Lorenz, R., Pitman, A. J., and Sisson, S. A.: Does Amazonian deforestation cause global effects; can we be sure? J. Geophys. Res. - Atmos., 121, 5567-5584. https://doi.org/10.1002/2015JD024357, 2016.

Lv, M. X., Ma, Z. G., Li, M. X., and Zheng, Z. Y.: Quantitative analysis of terrestrial water storage changes under the Grain for Green Program in the Yellow River basin, J. Geophys. Res. - Atmos., 124, 1336-1351, https://doi.org/10.1029/2018JD029113, 2019a.

Lv, M. X., Ma, Z. G., and Peng, S. M.: Responses of terrestrial water cycle components to afforestation within and around the Yellow River basin, Atmos. Ocean. Sci. Lett., 12, 116-123, https://doi.org/10.1080/16742834.2019.1569456, 2019b.

Miao, C. Y., Ni, J. R., and Borthwick, A. G. L.: Recent changes of water discharge and sediment load in the Yellow River basin, China, Prog. Phys. Geog., 34, 541-561, https://doi.org/10.1177/0309133310369434, 2010.

Mlawer, E. J., Taubman, S. J., Brown, P. D., Iacono, M. J., and Clough, S. A.: Radiative transfer for inhomogeneous atmospheres: RRTM, a validated correlated-k model for the longwave, J. Geophys. Res. - Atmos., 102, 16663-16682, https://doi.org/10.1029/97JD00237, 1997.

Myneni, R., Knyazikhin, Y., Park, T.: MCD15A2H MODIS/Terra+Aqua Leaf Area Index/FPAR 8-day L4 Global 500m SIN Grid V006 [MCD15A2H], NASA EOSDIS Land Processes DAAC, https://doi.org/10.5067/MODIS/MCD15A2H.006, 2015a.

Myneni, R., Knyazikhin, Y., Park, T.: MOD15A2H MODIS/Terra Leaf Area Index/FPAR 8-Day L4 Global 500m SIN Grid V006 [MOD15A2H], NASA EOSDIS Land Processes DAAC, https://doi.org/10.5067/MODIS/MOD15A2H.006, 2015b.

Peng, J., Chen, S. L., and Dong, P.: Temporal variation of sediment load in the Yellow River basin, China, and its impacts on the lower reaches and the river delta, Catena, 32, 135-147, https://doi.org/10.1016/j.catena.2010.08.006, 2010.

Perugini, L., Caporaso, L., Marconi, S., Cescatti, A., Quesada, B., de Noblet-Ducoudre, N., House, J. I. and Arneth, A.: Biophysical effects on temperature and precipitation due to land cover change, Environ. Res. Lett. 12, https://doi.org/10.1088/1748-9326/aa6b3f, 2017.

Piao, S. L., Yin, G. D., Tan, J. G., Cheng, L., Huang, M. T., Li, Y., Liu, R. G., Mao, J. F., Myneni, R. B., Peng, S. S., Poulter, B., Shi, X. Y., Xiao, Z. Q., Zeng, N., Zeng, Z. Z., and Wang, Y. P. Detection and attribution of vegetation greening trend in China over the last 30 years, Global Change Biol., 21, 1601-1609, https://doi.org/10.1111/gcb.12795, 2015.

Pitman, A. J., Avila, F. B., Abramowitz, G., Wang, Y. P., Phipps, S. J., and de Noblet-Ducoudre, N.: Importance of background climate in determining impact of land-cover change on regional climate, *Nat. Clim. Change*, 1, 472-475, https://doi.org/10.1038/NCLIMATE1294, 2011.

Quesada, B., Devaraju, N., de Noblet-Ducoudré, N., and Arnett, A.: Reduction of monsoon rainfall in response to past and future land use and land cover changes, Geophys. Res. Lett., 44, 1041-1050, https://doi.org/10.1002/2016GL070663, 2017.

Skamarock, W. C., Klemp, J. B., Dudhia, J., Gill, D. O., Barker, D. M., Duda, M. G., Barker, D. M., Huang, X. Y., Wang, W., and Powers, J. G.: A description of the advanced research WRF version 3, NCAR Tech. Note NCAR/TN-475+STR, 133pp, doi:10.5065/D68S4MVH, 2008.

Spracklen, D. V., Baker, J. C. A., Garcia-Carreras, L. and Marsham, J. H.: The Effects of Tropical Vegetation on Rainfall, Annu. Rev. Env. Resour., 43, 193-218, https://doi.org/10.1146/annurev-environ-102017-030136, 2018.

© Author(s) 2019. CC BY 4.0 License.

Sulla-Menashe, D., Gray, J. M., Abercrombie, S. P., and Friedl, M. A.: Hierarchical mapping of annual global land cover 2001 to present: The MODIS Collection 6 Land Cover product, Remote Sens. Environ., 222, 183-194, https://doi.org/10.1016/j.rse.2018.12.013, 2019.

Sun, Q. H., Miao, C. Y., Duan, Q. Y., and Wang, Y. F.: Temperature and precipitation changes over the Loess Plateau between 1961 and 2011, based on high-density gauge observations, Global Planet. Change, 132, 1-10, https://doi.org/10.1016/j.gloplacha.2015.05.011, 2015.

Tang, X., Miao, C. Y., Xi, Y., Duan, Q. Y., Lei, X. H., and Li, H.: Analysis of precipitation characteristics on the loess plateau between 1965 and 2014, based on high-density gauge observations, Atmos. Res., 213, 264-274, https://doi.org/10.1016/j.atmosres.2018.06.013, 2018.

Wang, S., Fu, B. J., GAO, G. Y., Yao, X. L., and Zhou, J.: Soil moisture and evapotranspiration of different land cover types in the Loess Plateau, China, Hydrol. Earth Syst. Sc., 16, 2883-2892, https://doi.org/10.5194/hess-16-2883-2012, 2012.

Wang, S., Fu, B. J., Piao, S. L., Lu, Y. H., Ciais, P., Feng, X. M., and Wang, Y. F.: Reduced sediment transport in the Yellow River due to anthropogenic changes, Nat. Geosci., 9, 38, https://doi.org/10.1038/NGEO2602, 2016.

Xiao, J. F.: Satellite evidence for significant biophysical consequences of the “Grain for Green” Program on the Loess Plateau in China, J. Geophys. Res. - Biogeo., 119, 2261-2275, https://doi.org/10.1002/2014JG002820, 2014.

Zhang, S. L., Yang, D. W., Yang, Y. T., Piao, S. L., Yang, H. B., Lei, H. M., and Fu, B. J.: Excessive afforestation and soil drying on China’s Loess Plateau, J. Geophys. Res. - Biogeo., 123 (3), 923-935, https://doi.org/10.1002/2017JG004038, 2018.

Zhao, T. B., Guo, W. D., and Fu, C. B.: Calibrating and evaluating reanalysis surface temperature error by topographic correction, J. Climate, 21, 1440-1446, https://doi.org/10.1175/2007JCLI1463.1, 2008.

Zhao, Y. F., Zhu, J., and Xu, Y.: Establishment and assessment of the grid precipitation datasets in China for recent 50 years, J. Meteorol. Sci., 34, 414-420, https://doi.org/10.3969/2013jms.0008, 2014.

https://doi.org/10.5194/hess-2019-397
Preprint. Discussion started: 15 August 2019
© Author(s) 2019. CC BY 4.0 License.

Tables

Table 1. Descriptions of datasets used in this study

Variable	Dataset	Time span available	Temporal resolution	Spatial resolution
Land cover	MCD12Q1	2001-2017	Yearly	500 m
LAI/FPAR	MCD15A2H	4th July, 2002 to present	8-day	500 m
LAI/FPAR	MOD15A2H	8th Feburary, 2000 to present	8-day	500 m
Albedo	GLASS	1981 to present	8-day	0.05°
Initial and boundary conditions for WRF	ERA-Interim	1979 to present	6 hour	0.75°
Surface air temperature	National Meteorological Information Centre	1961 to present	Monthly	0.5°
Rainfall	National Meteorological Information Centre	1961 to present	Monthly	0.5°
Slope	SRTM	—	—	3 second (about 90 m)

https://doi.org/10.5194/hess-2019-397
Preprint. Discussion started: 15 August 2019
© Author(s) 2019. CC BY 4.0 License.
Hydrology and Earth System Sciences Discussions
Open Access

Table 2. The International Geosphere-Biosphere Programme (IGBP) classification and class descriptions

Name	Value	Description
Evergreen Needleleaf Forests	1	Dominated by evergreen conifer trees (canopy >2m). Tree cover >60%.
Evergreen Broadleaf Forests	2	Dominated by evergreen broadleaf and palmate trees (canopy >2m). Tree cover >60%.
Deciduous Needleleaf Forests	3	Dominated by deciduous needleleaf (larch) trees (canopy >2m). Tree cover >60%.
Deciduous Broadleaf Forests	4	Dominated by deciduous broadleaf trees (canopy >2m). Tree cover >60%.
Mixed Forests	5	Dominated by neither deciduous nor evergreen (40-60% of each) tree type (canopy >2m). Tree cover >60%.
Closed Shrublands	6	Dominated by woody perennials (1-2m height) >60% cover.
Open Shrublands	7	Dominated by woody perennials (1-2m height) 10-60% cover.
Woody Savannas	8	Tree cover 30-60% (canopy >2m).
Savannas	9	Tree cover 10-30% (canopy >2m).
Grasslands	10	Dominated by herbaceous annuals (<2m).
Permanent Wetlands	11	Permanently inundated lands with 30-60% water cover and >10% vegetated cover.
Croplands	12	At least 60% of area is cultivated cropland.
Urban and Built-up Lands	13	At least 30% impervious surface area including building materials, asphalt, and vehicles.
Cropland/Natural Vegetation Mosaics	14	Mosaics of small-scale cultivation 40-60% with natural tree, shrub, or herbaceous vegetation.
Permanent Snow and Ice	15	At least 60% of area is covered by snow and ice for at least 10 months of the year.
Barren	16	At least 60% of area is non-vegetated barren (sand, rock, soil) areas with less than 10% vegetation.
Water Bodies	17	At least 60% of area is covered by permanent water bodies.

https://doi.org/10.5194/hess-2019-397
Preprint. Discussion started: 15 August 2019
© Author(s) 2019. CC BY 4.0 License.

Table 3. Description of the experiment design

Experiment	Land cover	*VEGFRC*	*LAI*	*α*	Simulation period
LC_{2001}	2001	2001	2001	2001	1^{st} May to 30^{th} Sep. for years from 1996 to 2015
LC_{2015}	2015	2015	2015	2015	1^{st} May to 30^{th} Sep. for years from 1996 to 2015
LC_{futr}	Artifically constructed land cover and land surface biogeophysical parameters (see text)				1^{st} May to 30^{th} Sep. for years form 1996 to 2015
$LCENS_{2001}$	2001	2001	2001	2001	From varying initial time (from 21^{st} April to 1^{st} May) to 30^{th} Sep. for the year 2001
$LCENS_{2015}$	2015	2015	2015	2015	From varying initial time (from 21^{st} April to 1^{st} May) to 30^{th} Sep. for the year 2001

https://doi.org/10.5194/hess-2019-397
Preprint. Discussion started: 15 August 2019
© Author(s) 2019. CC BY 4.0 License.
Hydrology and Earth System Sciences
Open Access
Discussions

Figures

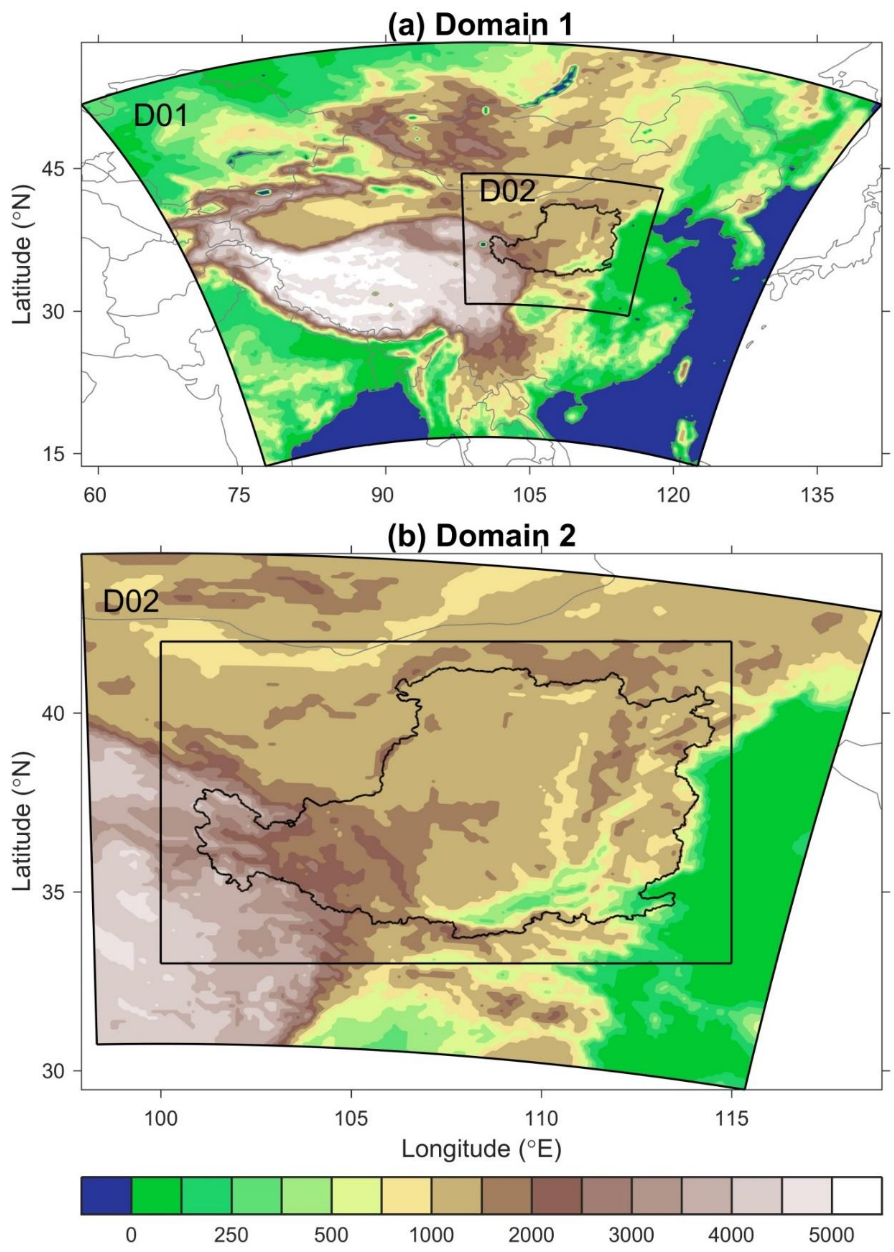

Figure 1. (a) The larger domain labelled D01 and (b) the inner nested domain labelled D02 configured for the WRF model. The topography (meters above sea level) is shown as colour shading. The Loess Plateau is enclosed by the black border. The black rectangle covers the region to be analysed in this study.

https://doi.org/10.5194/hess-2019-397
Preprint. Discussion started: 15 August 2019
© Author(s) 2019. CC BY 4.0 License.
Hydrology and Earth System Sciences
Open Access
Discussions

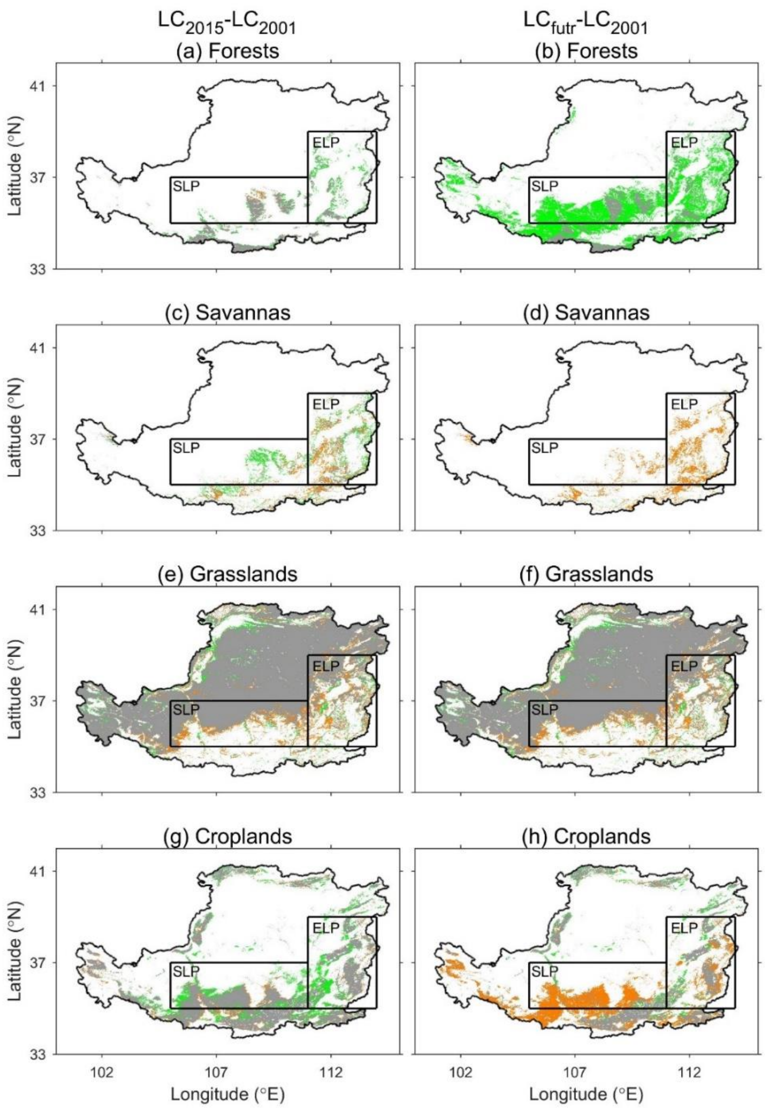

Figure 2. (a, c, e and g) Land cover changes between the LC_{2001} and LC_{2015} (LC_{2015}-LC_{2001}), and (b, d, f and h) between the LC_{2001} and LC_{futr} (LC_{futr}-LC_{2001}). The green, brown and grey colours denote the gained, lost and unchanged land cover respectively in the LC_{2015} (a, c, e and g) and LC_{futr} (b, d, f and h) compared with the LC_{2001}. Forests include evergreen needleleaf, evergreen broadleaf, deciduous needleleaf, deciduous broadleaf and mixed forests (see Table 2). Savannas include woody savannas and savannas. Croplands include croplands and cropland/natural vegetation mosaics. The south (105-111°E, 35-37°N) and east (111-114°E, 35-39°N) Loess Plateau are enclosed by black rectangles and labelled SLP and ELP respectively.

https://doi.org/10.5194/hess-2019-397
Preprint. Discussion started: 15 August 2019
© Author(s) 2019. CC BY 4.0 License.

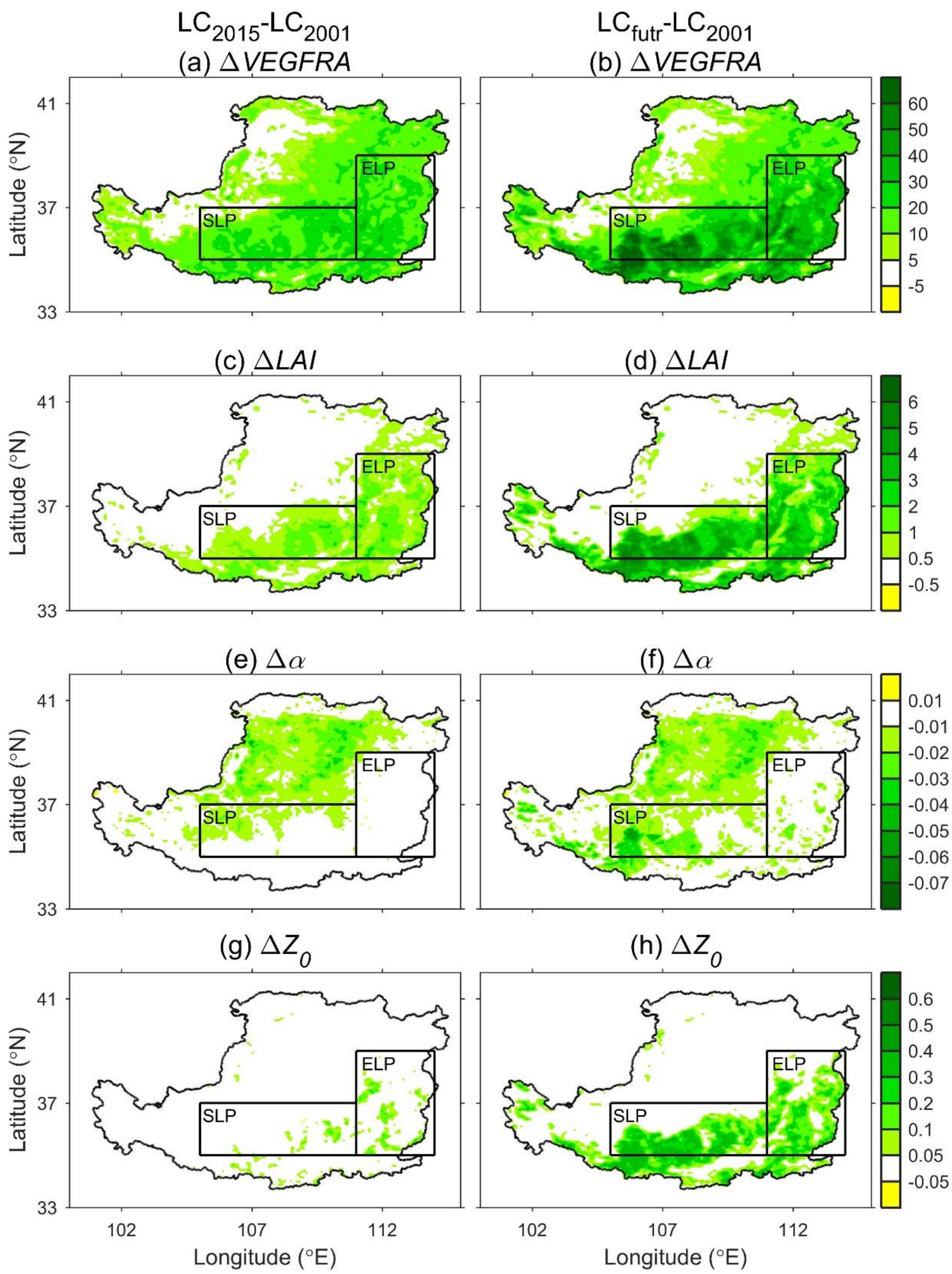

608

609 **Figure 3.** Changes in June-July-August-September mean (a and b) green vegetation fraction (%), (c and d) leaf

610 area index ($m^3 \cdot m^{-3}$), (e and f) albedo and (g and h) roughness length (m) between the LC_{2001} and LC_{2015} (LC_{2015}-

611 LC_{2001}; a, c, e and g), and between the LC_{2001} and LC_{futr} (LC_{futr}-LC_{2001}; b, d, f and h). The south (SLP) and east

612 (ELP) Loess Plateau regions are defined in Figure 2.

https://doi.org/10.5194/hess-2019-397
Preprint. Discussion started: 15 August 2019
© Author(s) 2019. CC BY 4.0 License.
Hydrology and Earth System Sciences
Open Access
Discussions

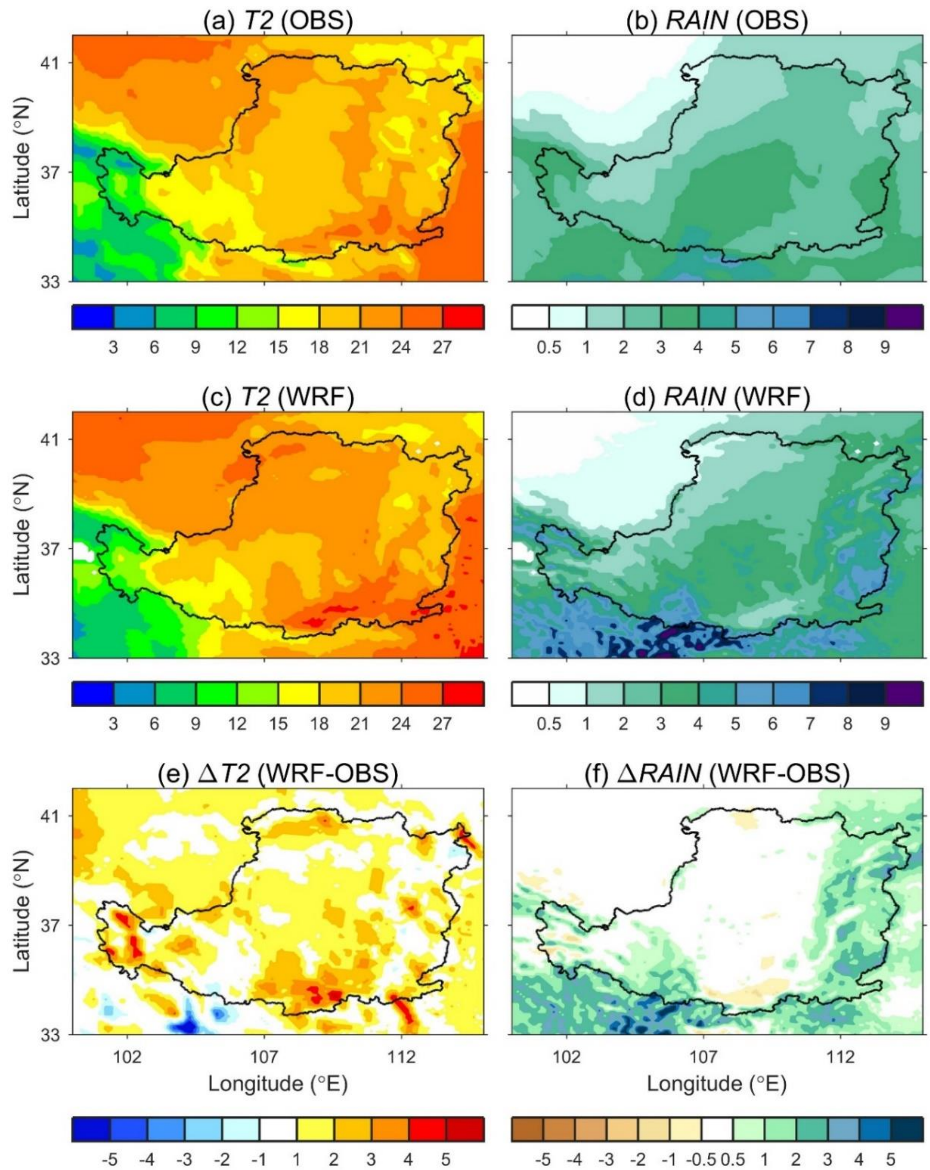

Figure 4. The WRF simulated June-July-August-September (JJAS) mean (a) surface air temperature (ºC) and (c) precipitation (mm·day^{-1}), and the observed JJAS mean (b) surface air temperature (ºC) and (d) precipitation (mm·day^{-1}) from the gridded observation dataset developed by the National Meteorological Information Centre of the China Meteorological Administration, and the differences in JJAS mean (e) surface air temperature (ºC) and (f) precipitation (mm·day^{-1}) between WRF simulations (WRF) and observations (OBS, WRF-OBS) over the Loess Plateau in 2001.

https://doi.org/10.5194/hess-2019-397
Preprint. Discussion started: 15 August 2019
© Author(s) 2019. CC BY 4.0 License.

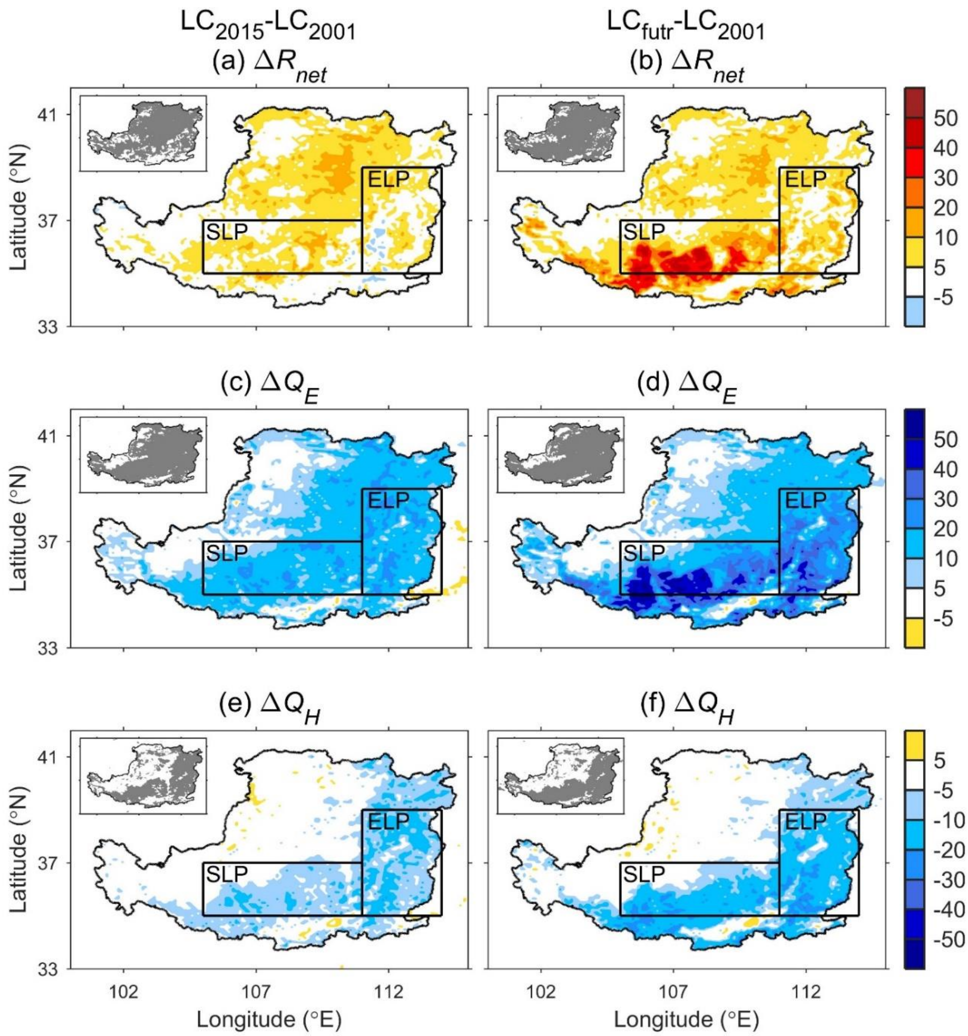

Figure 5. Changes in June-July-August-September mean (a and b) land surface net radiation (W·m^{-2}), (c and d) latent heat flux (W·m^{-2}) and (e and f) sensible heat flux (W·m^{-2}) between the LC_{2001} and LC_{2015} (LC_{2015}-LC_{2001}; a, c, and e), and between the LC_{2001} and LC_{futr} (LC_{futr}-LC_{2001}; b, d, and f). The south (SLP) and east (ELP) Loess Plateau regions are defined in Figure 2. The map of statistical significance test is shown in the embedded figure on the upper left corner of each panel. The grey denotes the local change is statistically significant at 95% confidence level using a two-tailed Student's *t*-test.

https://doi.org/10.5194/hess-2019-397
Preprint. Discussion started: 15 August 2019
© Author(s) 2019. CC BY 4.0 License.
Hydrology and Earth System Sciences
Open Access
Discussions

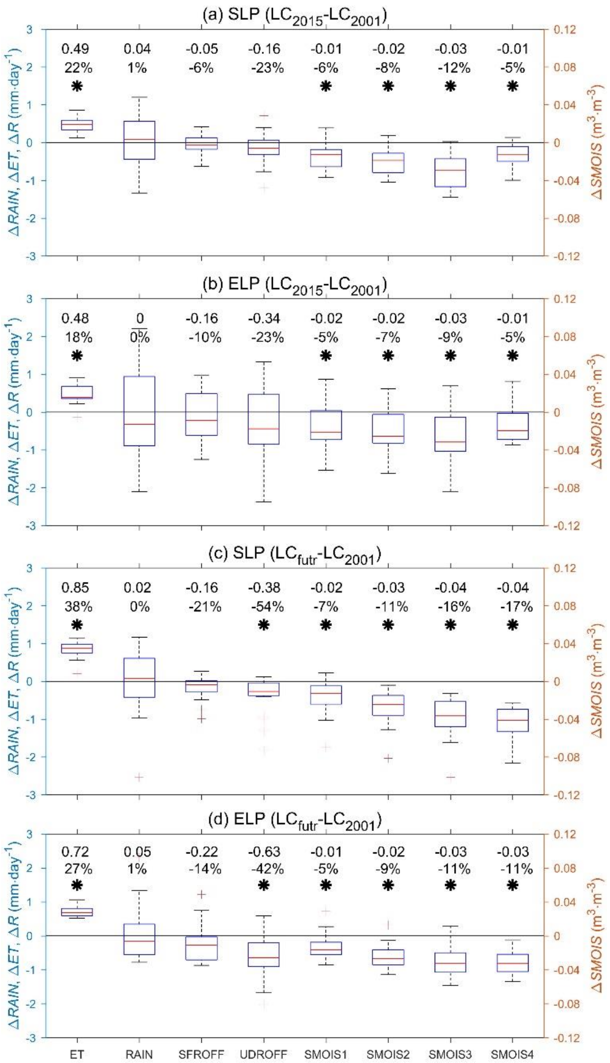

Figure 6. Box plot of changes in June-July-August-September mean evapotranspiration (*ET*, mm·day^{-1}), rainfall (RAIN, mm·day^{-1}), surface runoff (SFROFF, mm·day^{-1}), underground runoff (UDROFF, mm·day^{-1}) and soil moisture (m^3·m^{-3}) of 1st layer (*SMOIS1*, 0-10 cm), 2nd layer (*SMOIS2*, 10-40 cm), 3rd layer (*SMOIS3*, 40-100 cm) and 4th layer (*SMOIS4*, 100-200 cm) averaged over (a and c) south Loess Plateau and (b and d) east Loess Plateau between LC_{2001} and LC_{2015} (LC_{2015}-LC_{2001}; a and b), and between LC_{2001} and LC_{futr} (LC_{futr}-LC_{2001}; c and d). The south (SLP) and east (ELP) Loess Plateau regions are defined in Figure 2. The 1st and 2nd line members denote absolute and relative changes averaged by twenty members. The black asterisk denotes the change is statistically significant at 95% confidence level using a two-tailed Student's *t*-test.

https://doi.org/10.5194/hess-2019-397
Preprint. Discussion started: 15 August 2019
© Author(s) 2019. CC BY 4.0 License.
Hydrology and Earth System Sciences
Open Access
Discussions

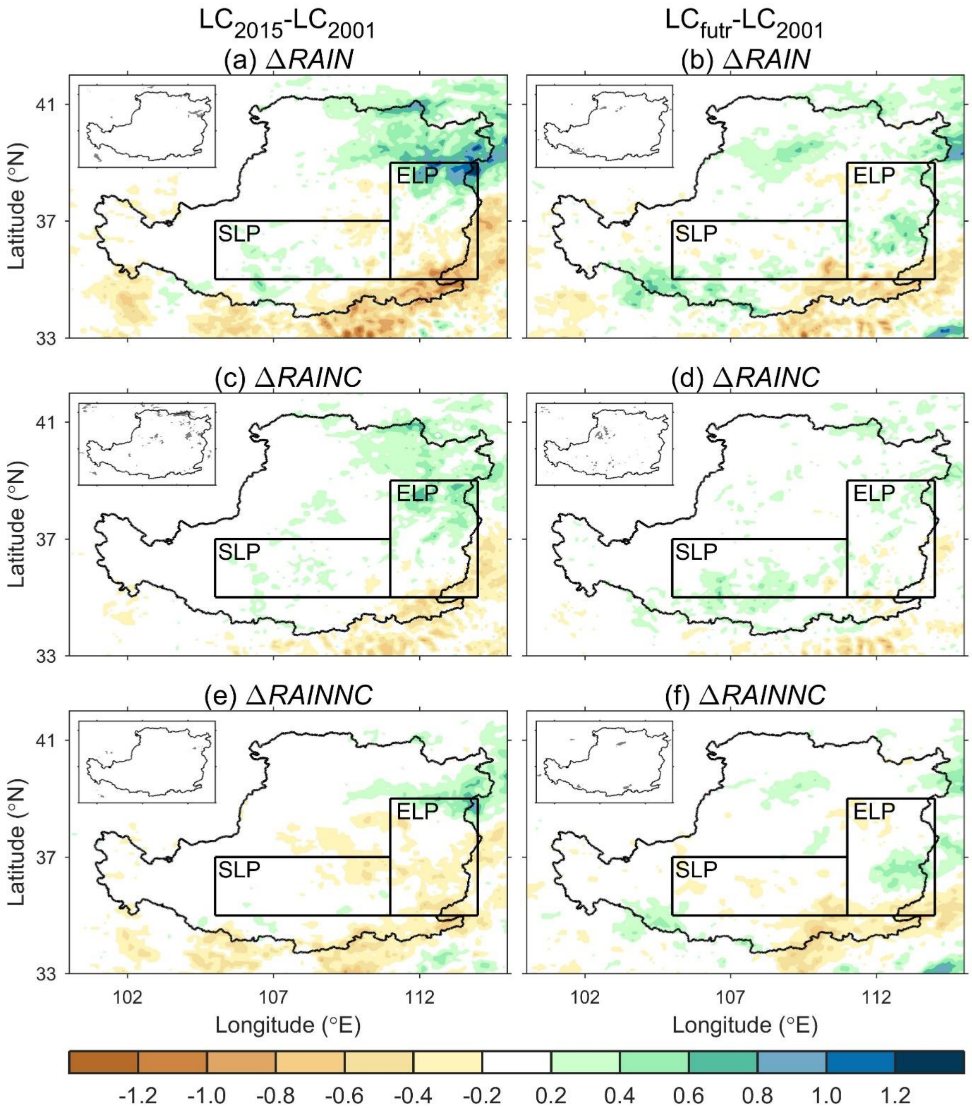

636

637 **Figure 7.** Same as Figure 5, but for (a and b) total rainfall (mm·day^{-1}), (c and d) convective rainfall (mm·day^{-1})
638 and (e and f) non-convective rainfall (mm·day^{-1}). The south (SLP) and east Loess Plateau (ELP) regions are
639 defined in Figure 2.

https://doi.org/10.5194/hess-2019-397
Preprint. Discussion started: 15 August 2019
© Author(s) 2019. CC BY 4.0 License.

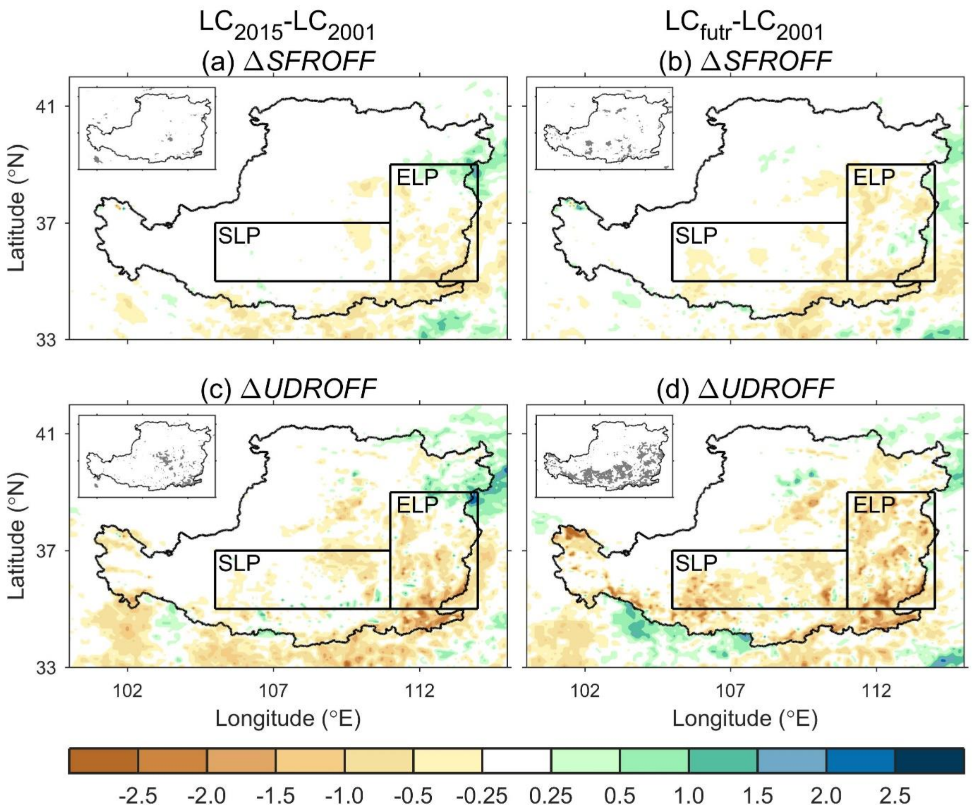

Figure 8. Same as Figure 5, but for (a and b) surface runoff (mm·day^{-1}) and (c and d) underground runoff (mm·day^{-1}). The south (SLP) and east Loess Plateau (ELP) regions are defined in Figure 2.

https://doi.org/10.5194/hess-2019-397
Preprint. Discussion started: 15 August 2019
© Author(s) 2019. CC BY 4.0 License.

Hydrology and Earth System Sciences
Open Access
Discussions

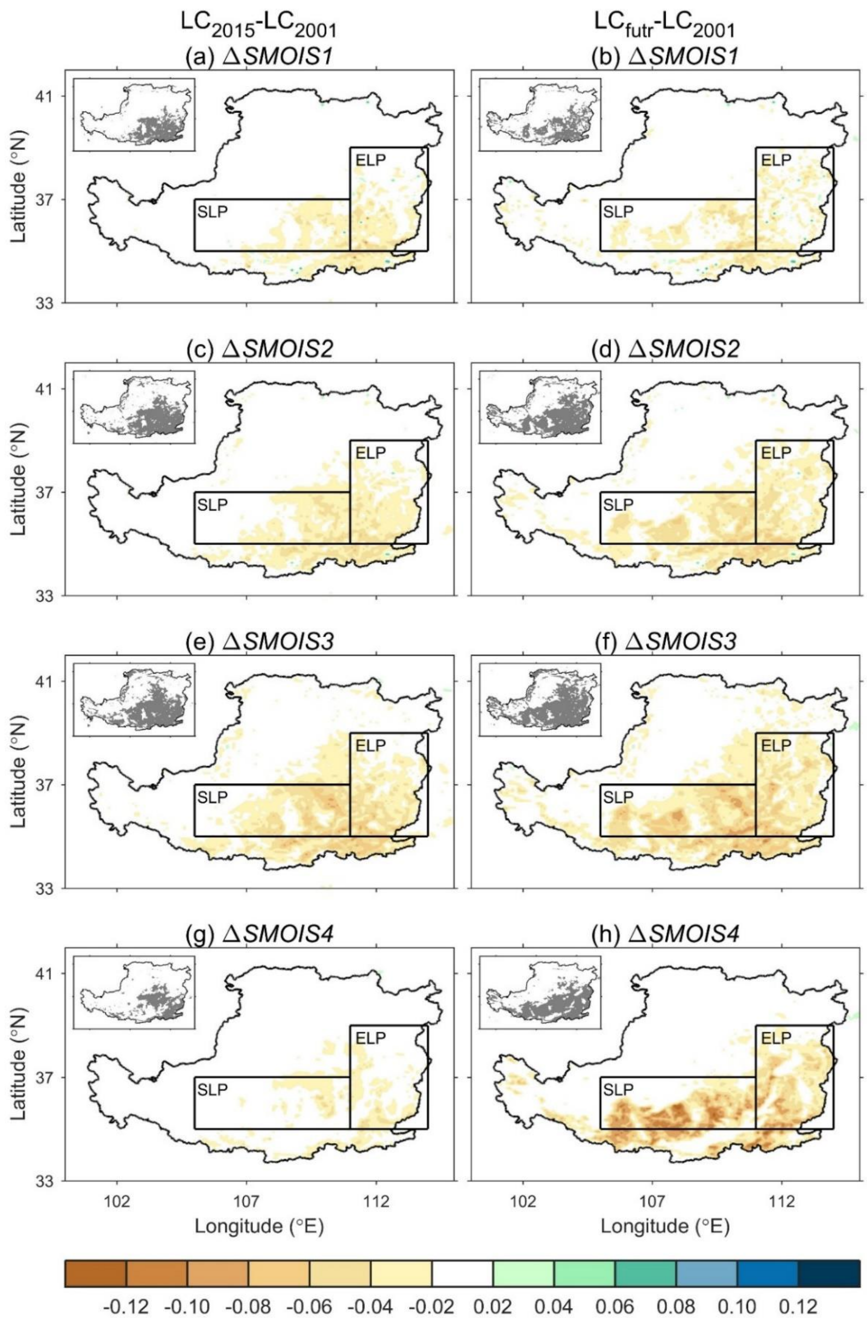

643

644 **Figure 9.** Same as Figure 5, but for the soil moisture change ($m^3 \cdot m^{-3}$) of (a and b) first layer (0-10 cm), (c and d)
645 second layer (10-40 cm), (e and f) third layer (40-100 cm) and (g and h) forth layer (100-200 cm). The south (SLP)
646 and east (ELP) Loess Plateau regions are defined in Figure 2.

https://doi.org/10.5194/hess-2019-397
Preprint. Discussion started: 15 August 2019
© Author(s) 2019. CC BY 4.0 License.

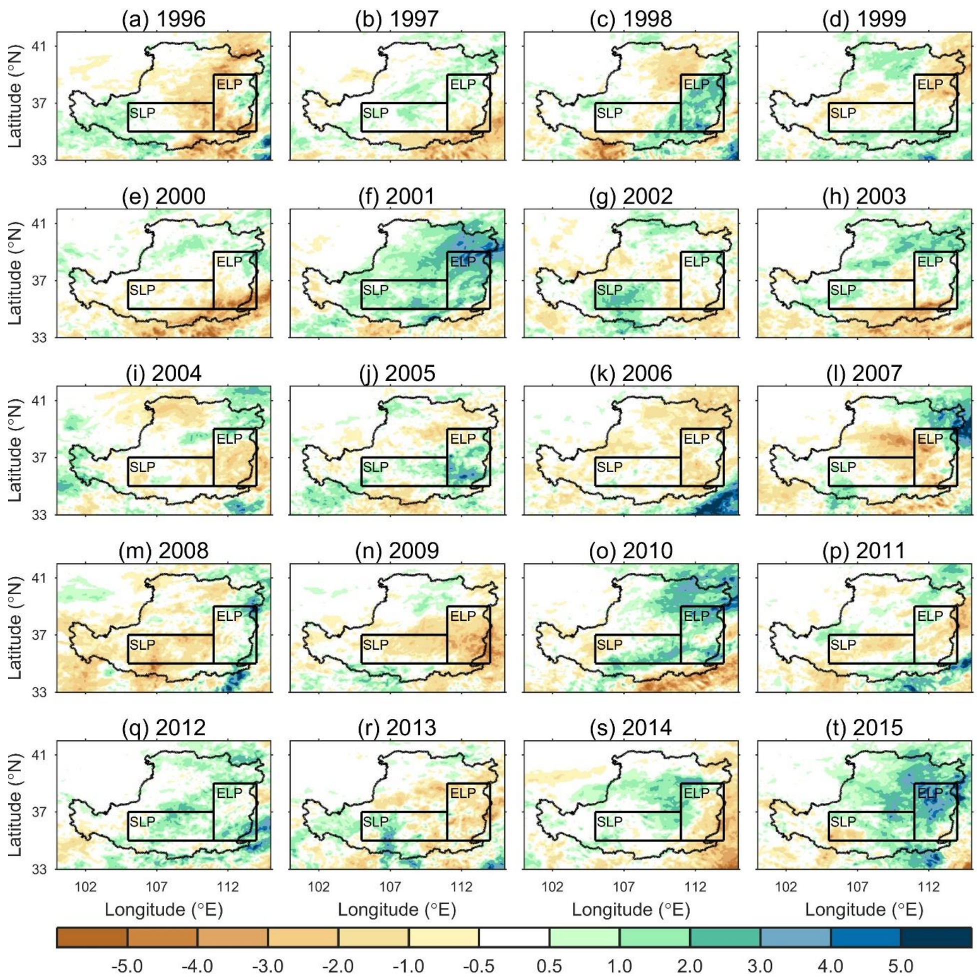

Figure 10. Changes in June-July-August-September mean rainfall (mm·day^{-1}) of each realisation members (years) between the LC_{2001} and LC_{2015} (LC_{2015}-LC_{2001}). The south (SLP) and east Loess Plateau (ELP) regions are defined in Figure 2.

https://doi.org/10.5194/hess-2019-397
Preprint. Discussion started: 15 August 2019
© Author(s) 2019. CC BY 4.0 License.

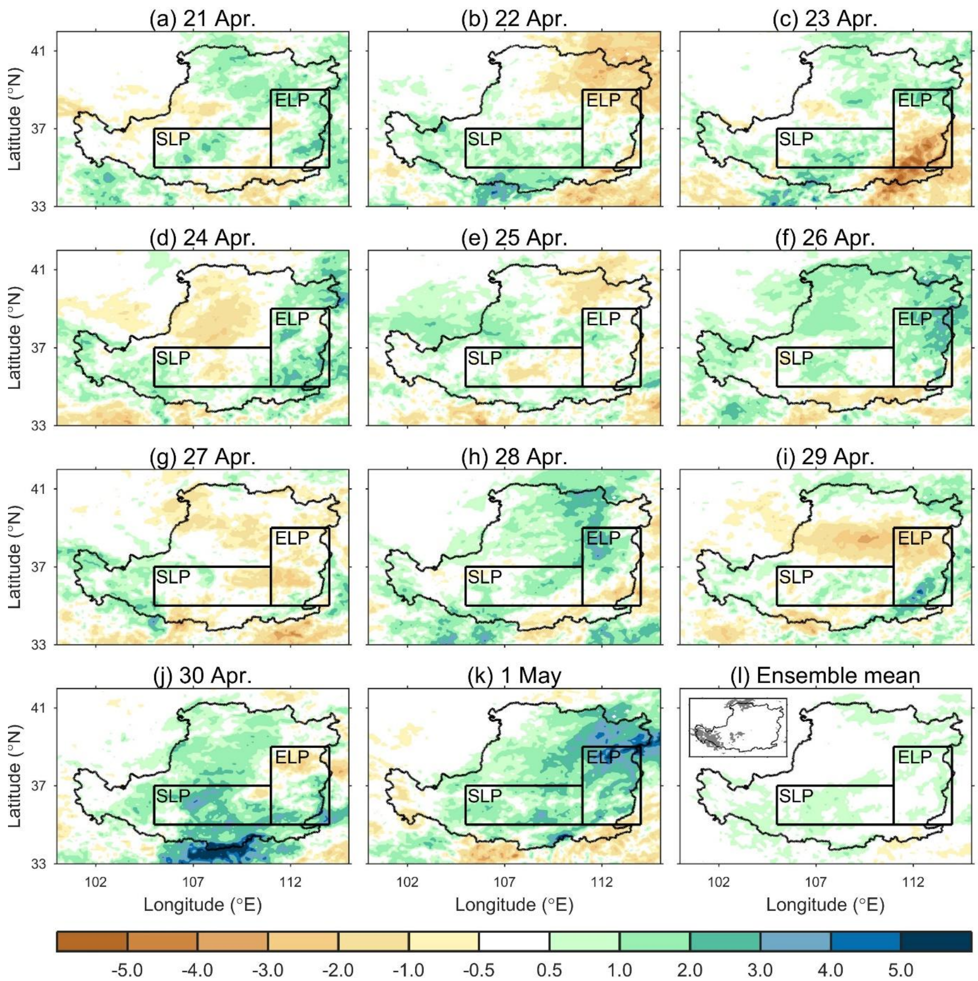

Figure 11. Changes in June-July-August-September mean rainfall (mm·day^{-1}) of each realisation member (a-k) and ensemble mean (l) between the $LCENS_{2001}$ and $LCENS_{2015}$ (LC_{2015}-LC_{2001}). The south (SLP) and east Loess Plateau (ELP) regions are defined in Figure 2. The map of statistical significance test is shown in the imbed figure on the upper left corner of panel l. The grey denotes the local change is statistically significant at 95% confidence level using a two-tailed Student's *t*-test.

https://doi.org/10.5194/hess-2019-397
Preprint. Discussion started: 15 August 2019
© Author(s) 2019. CC BY 4.0 License.

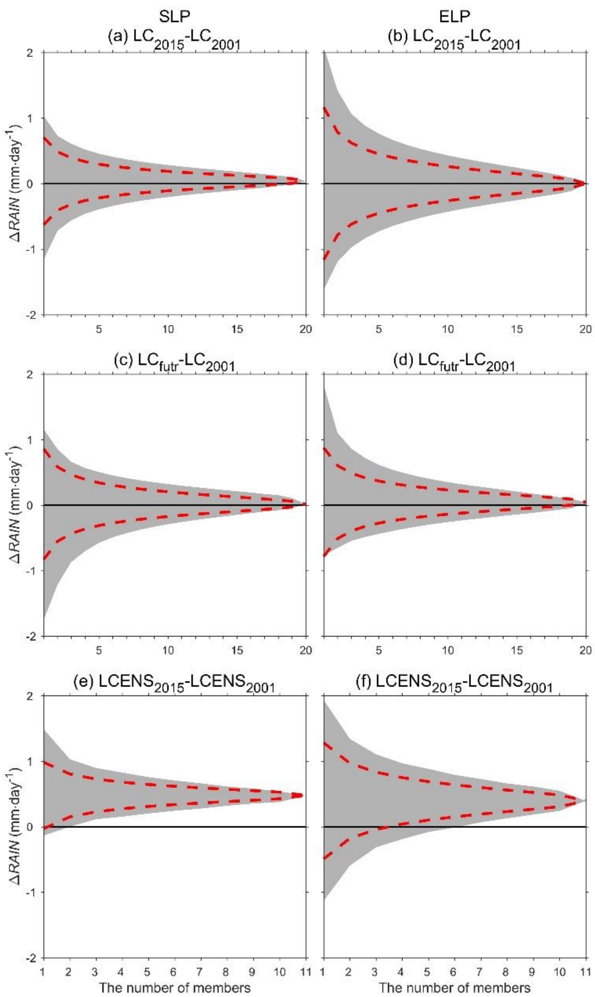

Figure 12. The relationship between the changes in June-July-August-September mean rainfall (mm·day^{-1}) and the number of members. The number of members ranges from 1 to 20 for (a and b) LC_{2015}-LC_{2001} and (c and d) LC_{futr}-LC_{2001}, and from 1 to 11 for (e and f) $LCENS_{2015}$-$LCENS_{2001}$. The mean rainfall change is averaged over (a, c and e) south Loess Plateau and (b, d and f) east Loess Plateau respectively. The south (SLP) and east (ELP) Loess Plateau regions are defined in Figure 2. For a given number of realisations, the rainfall is averaged over these members. The grey area denotes the range of rainfall changes from all possible combinations of a given number of members. The red dashed line denotes the 5th and 95th percentile of the rainfall changes from all possible combination of a given number of members.